UNIVERSITY OF
CAMBRIDGE
Department of Engineering

Rainfall-runoff Processes in Urban Environments

Fourth-year undergraduate project
in Group D, 2015/2016

Author Name: Pui Hei Lam (PEM)
Supervisor: Dr. Dongfang Liang

I hereby declare that, except where specifically indicated, the work submitted herein is my own original work.

Signed _____ *date* _____

Technical Abstract

Since the dawn of industrial revolution, urban population had grown in unprecedented rate. Many of these urban population booming occurred in places with abundant rainfall. As an area urbanized, vegetation and permeable soil would be replaced or covered by impermeable artificial materials such as concrete and asphalt. Without an efficient drainage system, water could easily accumulate under a heavy rain and cause flooding. Aggregated by fragile structures and mismanagement, casualties and property losses are likely. Therefore, in an attempt to avoid such adversities, it is important to understand the relationship between built-up areas and rain-induced flood.

Various attempts have been made in past researches to simulate flood and draw relationships between terrain and floods. One of the verified models was the shallow water equations, which have been adopted in this project. The two-dimensional shallow water equations with Total Variation Diminishing-MacCormack scheme allowed flood properties to be calculated.

Influences of building area ratio, building density and bed roughness on rainfall-induced flooding have been studied in the project. To proceed with the investigation, multiple variables are identified. Rainfall (i), surface gradient (s_b), catchment area (A) and bed roughness are varied, while buildings inserted in terrain with different patterns: regular, staggered or random. With each of the patterns, building area ratio and building density are then altered. Buildings are represented by the building-hole method, proven to be a suitable technique in previous researches. In addition to hydrological, topographic and building parameters, resolution and time step also affect accuracy and stability of simulation results.

Dimensional analysis has been used to generalize flow results for comparisons. By integrating the flow at the outlet of catchment, flow data are obtained against time. It has been found in previous research that dimensionless terms $\frac{Q_x}{it}$ and $\frac{t\sqrt{s_b \times g}}{A^{\frac{1}{4}}}$ are capable of generalizing flows and time in different simulation conditions, hence dimensionless S-curves can then be drawn. The time at which 70% of flow is reached is recorded, and benchmarked against different simulations. This has been done in view of the theoretical impossibility to simulate 100% flow in computation.

Having verified the effectiveness of dimensional analysis, influences of building area ratio, building density and bed roughness are analysed through application of the model. It

has been found in general, that increasing building area ratio, increasing building density and increasing bed roughness causes a lengthening time of concentration.

In investigating influence of building area ratio, 0, 5%, 10%, 20% and 30% of catchment area were tested in regular, staggered and random matrices. In investigating influence of building density, 25, 36, 64, 100, 144, 225 and 400 buildings were tested in regular, staggered and random matrices, maintaining topographic and hydrological conditions constant. In both investigations, it was found that the time of concentration increased in linear relationship in regular and random matrices, while it rose in quadratic relationship in staggered matrices.

In investigating influence of bed roughness, attempts were made to declare roughness in Manning coefficient or roughness height. It was found that Manning coefficient would give smoother flow response in the range of $n = 0.001m^{\frac{-1}{3}}s$ to $n = 0.05m^{\frac{-1}{3}}s$. In all building patterns, times of concentration increased with roughness in linear relationship.

The increase of time of concentration was due to a reduced velocity of flow in the catchment. With more buildings, water meandered through more obstacles, losing more energy as it hit the building surface or turned around at corners of buildings. Investigating deeper into the flow field, increasing building area ratio or density would build up the separation zone, narrowing the effective width of the flow path between buildings. This narrowing made channels not fully utilised. With increasing building area ratio or density, the aggregated effect of channel under-utilisation would be more pronounced; hence the time of concentration increased.

Simulations in the project had demonstrated capability of providing robust numerical solutions to floods under uniform continuous rainfall. The project also provided understanding of effects of building area ratio, building density, building pattern and bed roughness in urban flooding. With these effects in mind, further investigations could be made in the future to explore impacts of catchments in different shapes. This would help boost confidence for drainage designers to adopt research results in analysing and mitigating potential floods.

Contents

Technical Abstract i

Introduction 3

1. Background 3

2. Previous Research 4

3. Present Research 4

Objective 4

Theoretical Background 5

1. Number of Dimensions Used in Study 5

2. Shallow Water Equations 5

3. Numerical Scheme 6

4. Unit Hydrograph Theory 6

5. Dimensional Analysis and non-dimensional S-curve 7

Model Set-up and Verification 7

1. Parameters and Scope of Study 7

1.1 Computational Parameters 7

1.2 Overall Catchment Parameters 8

1.2.1 Time of Concentration 8

1.2.2 Time Steps and Simulation Domain 9

1.3 Building Matrices 10

2. Pre- and Post-Simulation Processing Methods 11

3. Model Verification and Normalisation of Results 11

3.1. Non-Dimensional S-curve 11

3.1.1 Regular Matrix 13

3.1.2 Random Matrix 15

Model Application 16

1. Choice of Resolution and Catchment 16

1.1 Choice of resolution 16

1.2 Choice of catchment 18
2. Influence of Building Area Ratio 21
2.1 Studied Cases 21
2.2 Non-dimensional S-curve and Time of concentration 23
2.3 Flow Field Examination 25
2.3.1 Explanation of increasing t_c with increasing BA 25
2.3.2 Explanation of staggered t_c crossing random t_c 28
3. Influence of Building Density 29
3.1 Studied Cases 29
3.2 Time of Concentration Graphs 30
3.3 Flow Field Examination 31
3.3.1 Explanation of increasing t_c with building density 31
3.3.2 Explanation of staggered t_c crossing random t_c 32
4. Influence of Bed Roughness 34
4.1 Studied Cases 34
4.2 Non-dimensional S-curve and Time of Concentration 35
4.3 Flow Field Examination 37
Conclusions 39
1. Conclusions 39
2. Future Work 41
Acknowledgements 42
References 42
Appendix 43
1. Risk Assessment Retrospective 43
2. Matlab Script for Building Matrix and Terrain Generation 44
3. Data of Random Matrix in Building Area Study (100 Buildings) 47
4. Data of Random Matrix in Building Area Study (64 Buildings) 48
5. Data of Random Matrix in Building Density Study 49

Introduction

1. Background

Urban population had ever been increasing since the dawn of industrial revolution. As of 2014, 54% of the global population resided in urban areas, up from 30% in 1950 and projected to grow to 66% by 2050. 90% of urban population growth was projected to happen in Africa and Asia. (United Nations, 2014) Accompanied by urbanization was increasing number of structures in urban areas. For low land price, low construction cost and no conflicts of occupancy, many of these structures were built on difficult terrains and constructed with cheap materials and insecure techniques. In addition, many of these cities were located in areas with abundant rainfall and frequent rainstorms. When seasonal heavy rainfall arrived, these poor structures would be very prone to collapse, causing casualties and property lost. Aggregated by extreme weather conditions induced by global climatic change, many heavily populated cities were prone to suffer.

Because of the heavy use of impermeable construction materials such as concrete and asphalt, little infiltration could occur in urban areas, causing flash flood to occur. Unlike rainfall in rural areas where infiltration and base flow could divert water to below ground, flash floods would cause water to accumulate above ground within a short period of time after the start of rainfall. Flooding disrupted daily lives and businesses, and even caused injuries and fatalities in serious incidents. Therefore, it was important to understand urban flooding, so that preventive measures such as embankment reinforcements and improved drainage system could be developed as part of damage mitigation.

Figure 1 Favela in Rio de Janeiro[1]

Figure 2 Rain-induced mudslide caused significant casualties in 2011 in Rio de Janeiro[2]

[1] Chensiyuan. (2010). inside rocinha favela rio de janeiro brazil 2010. Retrieved May 21, 2016, from https://commons.wikimedia.org/w/index.php?curid=14872516

[2] Lôbo, D. (2011). Floods in Brazil. Retrieved May 21, 2016, from http://water.thinkaboutit.eu/think5/post/floods_in_brazil

2. Previous Research

The pursuit of analytical solution to floods could be dated back for long. In Butler (1977) an attempt to generalize impacts of uniform excess rainfall on a unit width plane was made. Expressions of time of concentration in turbulent and laminar conditions were proposed and correlated to experimental data. In Govindaraju et al. (1990) sinusoidal solutions for kinematic waves were derived to approximate shallow water equations. The rising and falling limp of hydrographs were developed and shown comparable to numerical solutions of shallow water equations.

Cea et al. (2009) had attempted to compare results of two computational methods: dynamic and diffusive wave models with experimental results from laboratory configurations of urban catchments. It was found that the dynamic wave model gave more accurate predictions on the peak discharge, as well as generating an outlet hydrograph more similar to the experimental hydrograph. By using a similar model, researches had been done on establishing non-dimensional S-curves in urban flooding simulations. (Liang, Özgen, Hinkelmann, Xiao, & Chen, 2015)

3. Present Research

In view of increasing man-made structures in urban environments, the project aimed to enhance understanding of how buildings and surface roughness influence rain-induced floods. Several techniques such as dimensional analysis, computer simulations and regression aided the investigation. These techniques and application of techniques would be discussed further in details in later parts of the report.

Objective

The main objective of the project was to establish relationship between times of concentration of rain-induced flooding in urban environment with different building and terrain conditions. This was achieved by solving two-dimensional shallow water equations (2-D SWE) in set domains.

In the project, six effects will be explored: building area ratio, building density, bed roughness, rainfall intensity (i), surface gradient (s_b) and size of catchment (A, determined by grid size Δx). Previous researches had indicated that rainfall intensity (Gottardi & Venutelli, 2007), geometric boundaries (Cea, Garrido, & Puertas, 2009) and building layouts (Liang et al., 2015) were influential in time of concentration.

Theoretical Background

1. Number of Dimensions Used in Study

In choosing simulation models of different dimensions, since floods did not have clear flow paths like discharge in rivers, one-dimensional analysis would not be sufficient. On the other hand, as water depth of floods was expected to be orders of magnitude smaller than the size of catchment, it would be very difficult to construct a finite element mesh for simulation. A 10 mm deep flood would need at least 10 grid points in simulations. In catchments with side lengths up to 25 m, it was impossible to draw meshes with this wide aspect ratio. In addition, a 3-D solution would deem not feasible because the computational cost of running the model and data needed to build the 3-D model was huge. (Cea et al., 2009) Therefore, three-dimensional model was not suitable.

To allow computation of flows in two directions and fine meshes to be drawn, a two-dimensional model, 2-D Shallow Water Equations was adopted in the project.

2. Shallow Water Equations

The 2-D Shallow Water Equations (2-D SWE) comprised three equations, observing the conservation of mass (Equation 1) and conservation of momentum in x-direction (Equation 2) and y-direction (Equation 3). The SWE discarded effects of wind, Coriolis and viscous forces. In 2-D SWE analysis, the three independent variables investigated are velocities in x and y directions (u_x, u_y) and water depth above datum η, varying with time and position.

$$\frac{\partial \eta}{\partial t} + \frac{\partial q_x}{\partial x} + \frac{\partial q_y}{\partial y} = 0 \qquad \textit{Equation 1}$$

$$\frac{\partial q_x}{\partial t} + \frac{\partial (\frac{\beta {q_x}^2}{H})}{\partial x} + \frac{\partial (\frac{\beta q_x q_y}{H})}{\partial y} = -gH\frac{\partial \eta}{\partial x} - \frac{g q_x \sqrt{{q_x}^2 + {q_y}^2}}{H^2 C^2} \qquad \textit{Equation 2}$$

$$\frac{\partial q_y}{\partial t} + \frac{\partial (\frac{\beta q_x q_y}{H})}{\partial x} + \frac{\partial (\frac{\beta {q_y}^2}{H})}{\partial y} = -gH\frac{\partial \eta}{\partial y} - \frac{g q_y \sqrt{{q_x}^2 + {q_y}^2}}{H^2 C^2} \qquad \textit{Equation 3}$$

The adoption of 2-D SWE was based on the assumption that water depth was small in urban flooding so that vertical momentum exchange was insignificant. In all simulations water flow was unlikely to exceed 50 mm, which satisfied the assumption. By choosing the

building-hole method in computational simulation (to be described in section *Model Set-up and Verification*), rain water fallen on building roofs would be discarded from analysis.

3. Numerical Scheme

The 2-D SWE would be solved by an explicit Total Variation Diminishing-MacCormack scheme proposed by Liang et al. (2006). It was a scheme that "includes the addition of a five-point symmetric total variation diminishing (TVD) term to the corrector step of the standard MacCormack scheme." (Liang, Lin, & Falconer, 2006), allowing an efficient, conservative and accurate form of SWE to be calculated. Flexibility of using a variable time step by controlling the Courant number was also offered with this scheme. The model was verified in previous researches in dam breaking and extreme flooding scenarios. Further details could be found in Liang et al. (2006).

4. Unit Hydrograph Theory

The 2-D SWE solution was based on the theory that a duration of uniform rainfall would result in a certain discharge pattern. If the uniform rainfall lasted indefinitely, discharge at the outlet of catchment would reach saturation at a time of concentration (Tc). In other words, Tc was the parameter that categorized the rise of S-curve. The idea was captured by hyetographs and S-curve in Figure 3.

Comparing with rural area that was covered by rough surfaces, flooding in urban areas were likely to result in a quick rise in S-curve. This was because surfaces paved with asphalt and concrete were relatively smooth. Little resistance was offered. In the *Model Application* section, effects of surface roughness to time of concentration were demonstrated.

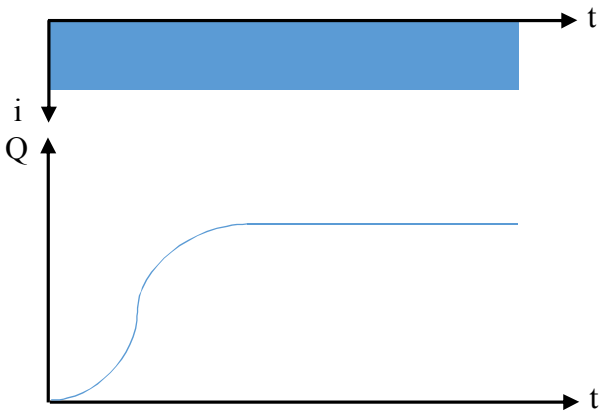

Figure 3 Hyetograph and S-curve of continuous uniform rainfall

5. Dimensional Analysis and non-dimensional S-curve

Raw data obtained from simulations or water experiment table were specific to the domain used. In order to facilitate comparison of data from different catchment domains, dimensional analysis was adopted in the hope of capturing generalised relationship. With unit hydrograph theory, under continuous rainfall the outflow should saturate at the volume of rainfall received in catchment at the time of concentration. If the rainfall received in catchment was normalised to a scale of 0 to 1, then all curves should collapse onto S-curves that levelled off at 1 at a dimensionless time of concentration. This would be verified in the first part of my project.

Dimensionless units were found in previous research (Liang et al., 2015) for direct comparison of results and better generalisation of relationships. S-curve produced for this project will have dimensionless flow $\frac{Q_x}{it}$ on the y-axis, versus dimensionless time $\frac{t\sqrt{s_b \times g}}{A^{\frac{1}{4}}}$ on x-axis (i – rainfall intensity in m/s, t – time in s, s_b – surface gradient, g – gravity in ms^{-2}, A – area of catchment for square catchments in m^2). The reason of not including a friction term in time of concentration was due to the assumption of frictionless flow in previous research. This assumption could be justified because most urban environment was paved with impermeable, smooth materials such as asphalt. In *Model Application* section, the effect of bed roughness was analysed. Further explanation could be found in Liang et al., 2015.

Model Set-up and Verification

1. Parameters and Scope of Study

All simulations were conducted with a previously verified 2-D SWE programme written by Dr. D. Liang. Hydrological conditions, topographic details and building configurations were inputted into the programme, returning with flow data that allowed graphics and calculations of time of concentration to be made.

To be investigated in the project were the influences of Building Area Ratio, Building Density and Bed Roughness to the times of concentration.

1.1 Computational Parameters

The following parameters were set as variables in the simulations:

Hydrological

Rainfall Intensity (i):	measured in m/s in programme, commonly displayed as mm/s for convenience

Topographic

Surface Gradient (s_b):	$\frac{Height\ difference\ of\ Catchment}{Length\ of\ catchment\ in\ principal\ direction\ of\ flow}$
Size of Catchment (A):	determined by resolution multiplied by grid size Δx.

Buildings

Building Area Ratio (BA):	$\frac{Building\ Area}{Catchment\ Area}$
Building Density:	$\frac{Number\ of\ Buildings}{Catchment\ Area}$, very often just denoted as number of buildings throughout the report, because most investigations were done in the same catchment with the same hydrological and topographic condition (i=1 mm/s, s_b=0.01, A=23.6196m^2 $(4.86m \times 4.86m)$)
Bed Roughness:	Chezy coefficient (C), manning's coefficient (n) and roughness height (ks) were used
Building Patterns:	Regular, Staggered, Random, Plain

1.2 Overall Catchment Parameters

1.2.1 Time of Concentration

In theory, it would take infinite time for the flow to actually reach 100% saturation. This requirement would be prohibitive to computational simulations. As an attempt to bypass the need of infinite time, in previous researches time to reach 25% of saturated (t_{25}) or 50% of saturated flow (t_{50}) had been used to characterize times of concentration (t_c). As long as comparisons were made based on the same percentage of flow, the results would still be valid. In this project, time reaching 70% of saturated flow (t_{70}) would be used instead. 70% was adopted in light of scenarios often having sharp rise of flow in the beginning of simulation. With finite interval between each record to minimise influence of noise, interpolation of t_c could only be made between two distant points. When comparing t_c from interpolated results, numerical error may compromise the actual differences caused by the variable, which was not beneficial. A bigger range of time required to reach 70% of saturated flow was observed through various simulations. This would benefit the comparison of t_c, hence t_{70} was adopted.

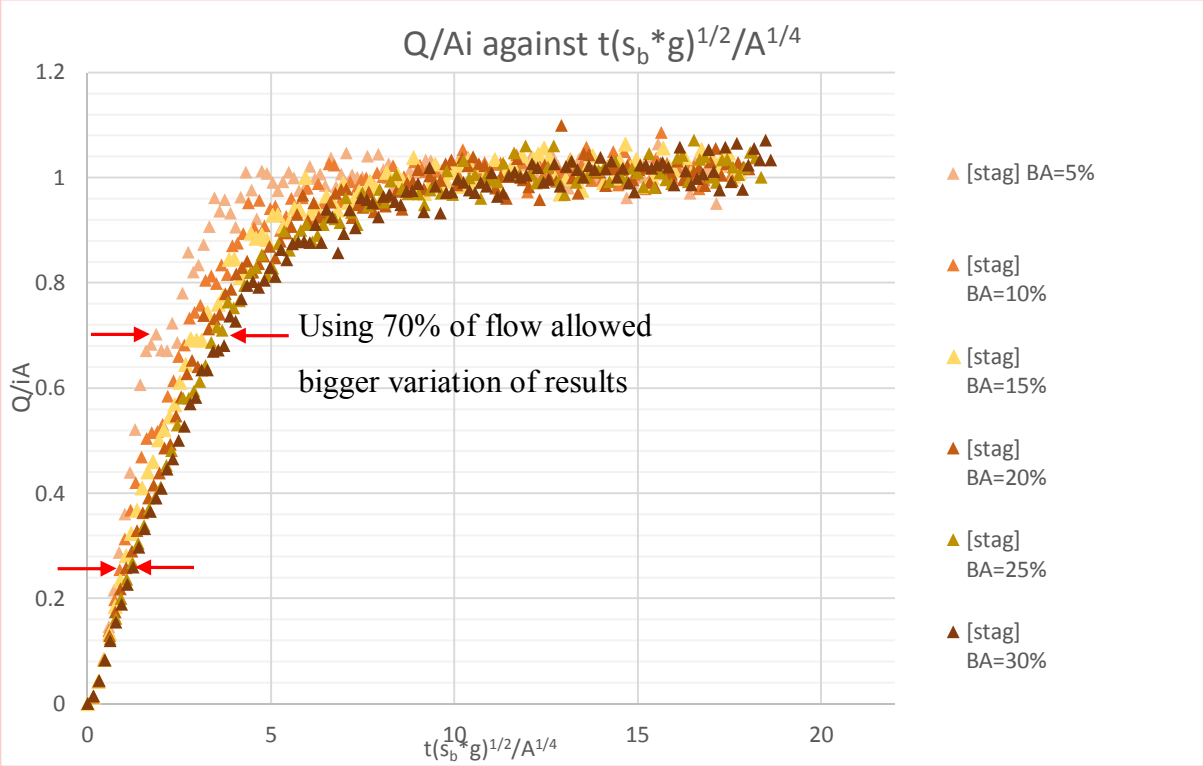

Figure 4 Plot of Dimensionless Flow over Time (Staggered matrix, 100 buildings, i=1mm/s, sb=0.01, dx=0.02m)

1.2.2 Time Steps and Simulation Domain

In the input, time steps were defined. It could be made variable to allow difficult step to be solved in smaller time steps but in almost all scenarios fixed time steps were adopted. This better controlled computational resources used, plus a limit of $\frac{\Delta x}{(\sqrt{gh}+|v_{max}|)}$ already provided robust control to each time step forward.

Simulation domains contained a square catchment followed by a water expulsion leeway of higher gradient. Domain sizes were defined by number of grid points multiplied by grid size. Three resolutions of grid points were used in the project: 1x had a catchment of 243 by 243 grid points; 2x had a catchment of 486 by 486 grid points; 4x had a catchment of 972 by 972 grid points. Higher resolutions were used to enable more accurate simulations and in some cases necessary, as to be suggested in Choice of Resolution in *Model Application* section. Very often when higher resolutions were pursued, the time difference had to be halved, as Δx term in the governing limit was halved.

The grid size (Δx) was self-defined to vary the catchment size for investigation. In previous research, Δx of 0.01 m, 0.02 m, 0.03 m, 0.05 m and 0.1 m were used to vary the catchment size. The effect of catchment size was captured by the dimensionless time term and it was verified to not cause a difference in times of concentration.

1.3 Building Matrices

As previous research proposed, in this project buildings would be computed by the building-hole method (BH) (Cea et al., 2009). In essence, buildings were represented as blocks in the domain and were exempted from computation. No rainfall would be fallen on buildings, nor water will flow across buildings. In addition to exemption from simulation, in the project buildings were also raised to 10m above datum level. This was to avoid water from flowing into building boundaries, as what would happen if they were kept at the same elevation as the surroundings. Although water originally fallen onto building roofs were not taken account of with BH, previous research had shown that prediction by this method closely matched experimental results. 2-D assumption was still valid even at the proximity of buildings with BH.

Codes were developed to generate building matrices in regular, staggered and random layouts for computer simulations. This enabled the research team to investigate influences of building patterns with times of concentration, from buildings with distinguishable straight flow path (regular), to pre-defined meandering flow path (staggered) and completely randomised flow path (random). For the purpose of this project, buildings were assumed to be squares, instead of rectangular as previous experiments adopted. Building sizes, number of buildings and building pattern could be defined by users.

Staggered matrices were aimed to look identical when viewed from the x-axis or the y-axis. Equidistance from centres of buildings was attempted, but it was found that such matrices cannot be symmetrical in x and y direction, while fitting onto a square catchment at the same time. A compromise was made so that separations between rows and columns of buildings remained the same in x and y direction. Admittedly, because of its staggered configuration, it would not be able to maintain the same number of buildings and building area ratio as regular or random matrices. The closest combination of building size and number would be adopted to allow fair comparison between staggered and other building patterns.

Random matrices were produced by using a built-in random number generator in Matlab. The generator assumed a uniform distribution from 0 to 1. After the number was generated, it would be multiplied by the catchment length minus the width of building (both specified by user) to find its x and y coordinate. Buildings were then assigned to random locations in the domain.

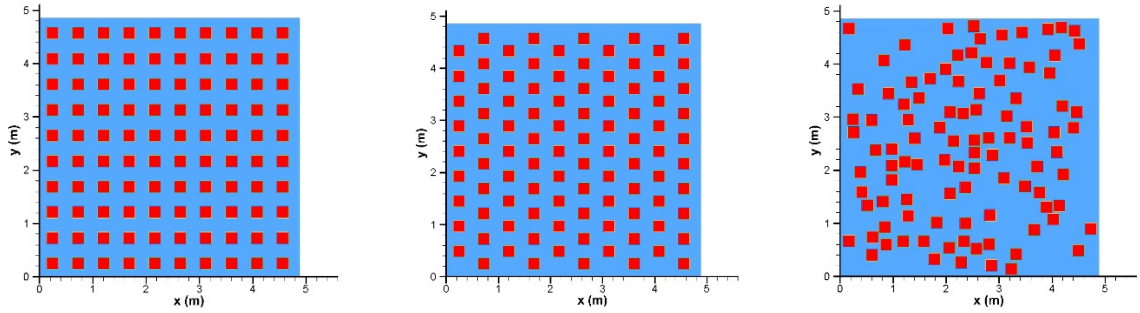

Figure 5a,b,c Regular, Staggered and Random matrices (BA=20%, 100 buildings)

2. Pre- and Post-Simulation Processing Methods

Before the simulation, building configuration and topographic conditions were defined and generated with an in-house script written in Matlab. The script required information of size of buildings, number of buildings, building pattern, gradient, size and bed roughness of catchment. The script could be found in the appendix. With results from Matlab, details of rainfall, domain size, building configuration and topographic conditions were inputted to standardized data files.

After simulation, data would be visualised and analysed by the software package. In this report, pictures of domains would have red blocks representing buildings and blue surface representing the flow terrain, unless otherwise stated. All domains shown were the catchment area; the water expulsion leeway was blanked out as it was not the component that affected results.

Time of concentration were determined by the flow at the end of the catchment. After integration by Tecplot, data would be obtained to get the dimensionless time required to reach 70% of saturated flow.

3. Model Verification and Normalisation of Results

3.1. Non-Dimensional S-curve

With methods described in section 2, shallow water equations were computed with inputted parameters. Computed results such as flow velocity and water depths were then visualised by visualisation software package and flows at the end of catchments were integrated.

The visualisation package allowed coloured flow diagrams to be shown. Different cases were used for verification and investigation, including the one shown in Figure 6 and Figure 7. Scenario the two figures were captured from was a verification case of BA=24.5%,

100 buildings, regular pattern, i=1mm/s, s_b=0.01, dx=0.02m. They were captured at 8 seconds and 19 seconds of simulation respectively.

The backdrop colour in catchment showed the water depth, while the arrows indicated the unit width flow rate at the grid point. As the colour leaned towards the red side of the rainbow spectrum and as the arrows enlarged, water depth and flow rate increased. With visual inspection it could be observed that as time progressed, under continuous uniform rainfall, water depth and flow rate increased. Flow rate could then be calculated at the end of catchment; in the figures the end of catchment was the right hand edge of the simulation domain. Output numbers could then be processed and plotted in graphs. As shown in Figure 8, t=8 seconds and t=19 seconds corresponded to the time when flow reached 40% and 90% of the saturated value. By reading off from the graph when the flow reached saturation, or for the purpose of this project the time when flow reached 70% of saturation, comparisons could be made on how buildings and bed roughness influenced the flow.

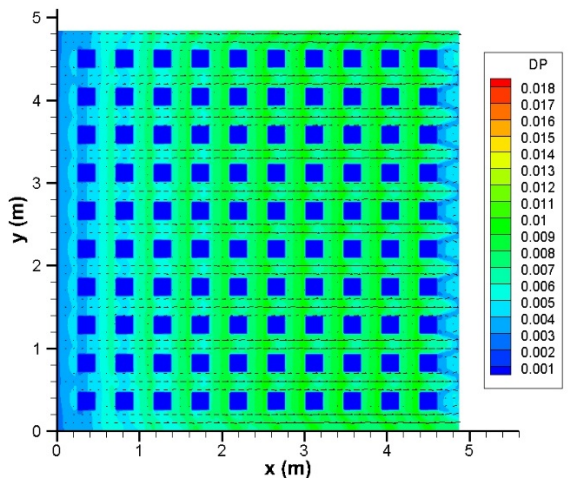

Figure 6 Flow and water depth (BA=24.5%, 100 buildings, regular, i=1mm/s, sb=0.01, dx=0.02m at t=8s)

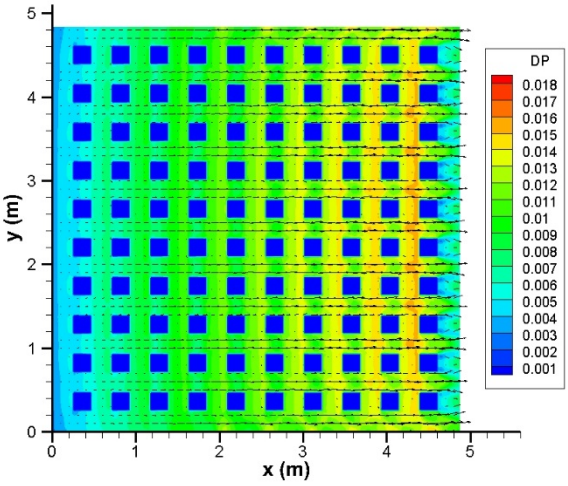

Figure 7 Flow and water depth (BA=24.5%, 100 buildings, regular, i=1mm/s, sb=0.01, dx=0.02m at t=19s)

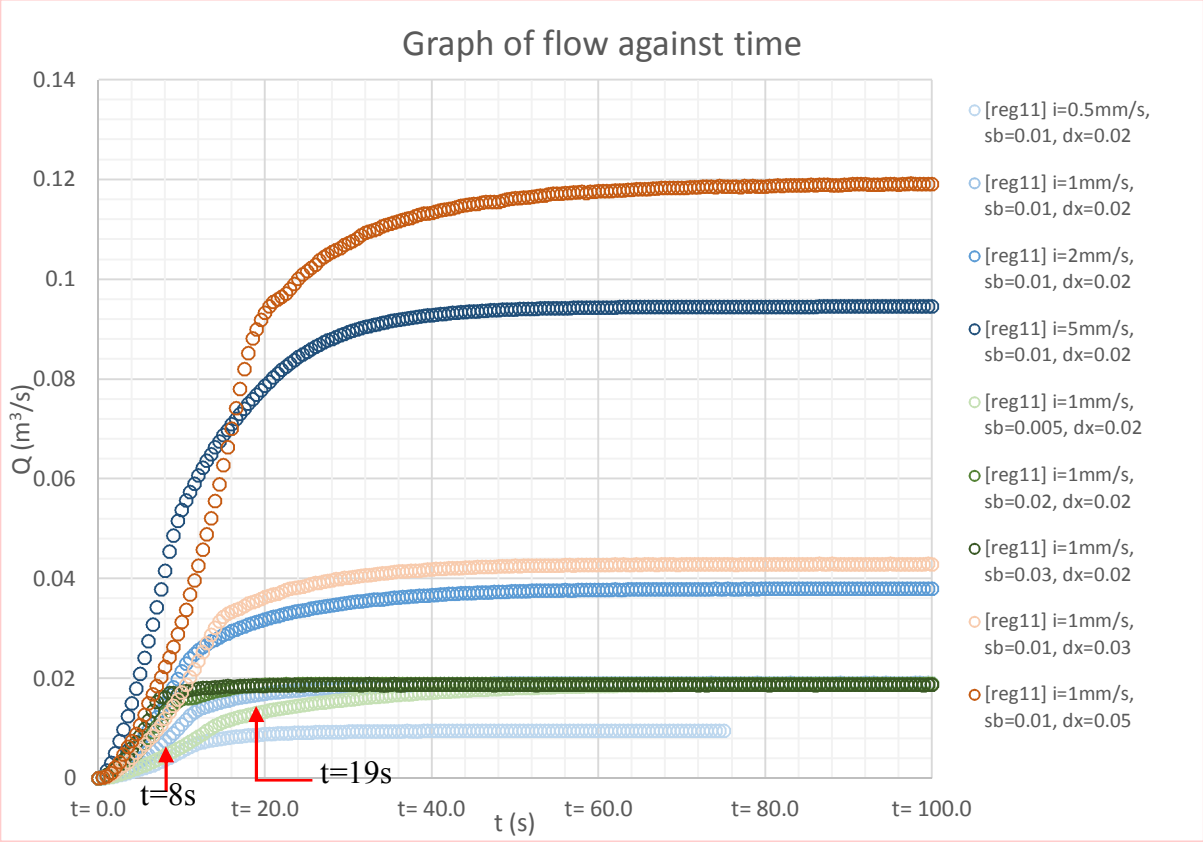

Figure 8 Graph of flow against time before dimensional analysis, verification cases

With the same technique, different parameters were inputted to the computation model for different flow results. The integrated flow rates were then plotted against time. With different area of catchment and rainfall intensity, different saturation flow rates were expected, as shown in Figure 8. This would increase difficulty in generalizing results and deriving relationships. Therefore, dimensional analysis was adopted and dimensionless information was obtained, as discussed in the next section.

3.1.1 Regular Matrix

As the first part of the verification process, simulations were done on 1x resolution, 10x10 regular building matrices at BA=24.5% and at very high Chezy coefficient ($C = 1 \times 10^{30}\ m^{\frac{1}{2}}s^{-1}$), creating a frictionless environment. Catchment size, rainfall intensity and surface gradient were varied; combinations were as follows:

Grid Size Δx (Affecting A): 0.02 m, 0.03 m, 0.05 m, 0.1 m

Rainfall intensity i: 0.5 mm/s, 1 mm/s, 2 mm/s, 5 mm/s

Surface Gradient (s_b): 0.005, 0.01, 0.02, 0.03

It could be shown in Figure 9 that with the use of dimensionless terms, times of concentration were consistent for different A, i and s_b.

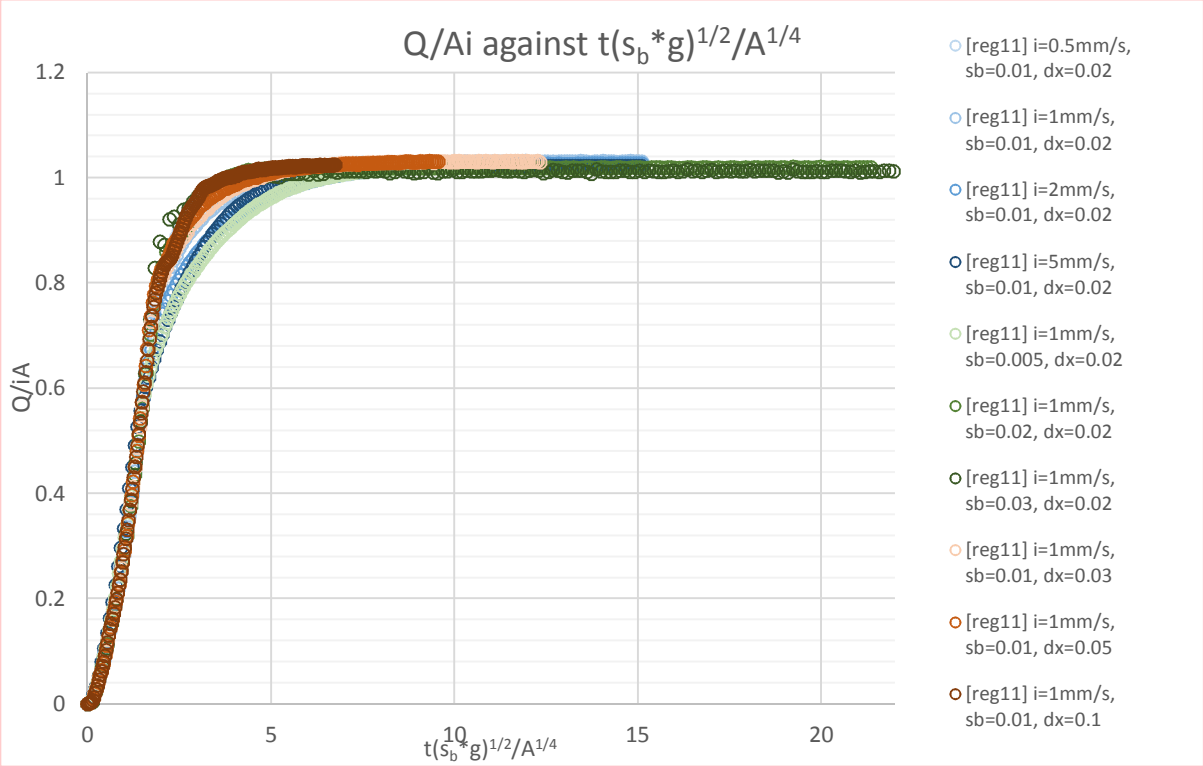

Figure 9 Dimensionless Flow against Dimensionless Time (Verification, regular matrix)

Constraining Water Depth

In situations of big catchment area and low rainfall intensity, serious fluctuations of flow rate were observed. Its flow condition was shown in Figure 10. The fluctuation was a result of water depth reaching the dry/wet threshold, toggling the grid point on and off and causing instability. Instability would cause water outflow at the catchment boundary to fluctuate significantly, and such fluctuation did not come from physical phenomena such as vortices at the ends of buildings.

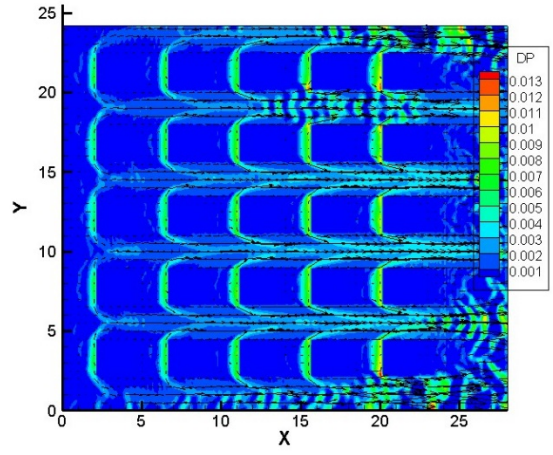

Figure 10 Instability caused by low water depth

As learned from verification, the minimum depth of water had to be at least 10mm over the majority of the catchment domain in order to ensure a stable simulation result. To avoid this computational error, instability could be alleviated by using a lower dry/wet threshold and minimum water depth, or introducing viscosity in simulations. For critical situations, fluctuation of outflow

was however inevitable, so scenarios of low rainfall intensity and high grid point intervals could only be avoided.

3.1.2 Random Matrix

Random matrices were tested in the second part of verification. Hydrological and topographic conditions were kept the same as the first verification. The only difference was changing the 10x10 regular matrix into 100 randomly distributed buildings. The building configuration used could be seen in Figure 12.

It could be shown that with the use of dimensionless terms, times of concentration were statistically consistent for different A, i and s_b. This was held true not only with regular matrices but also with random matrices.

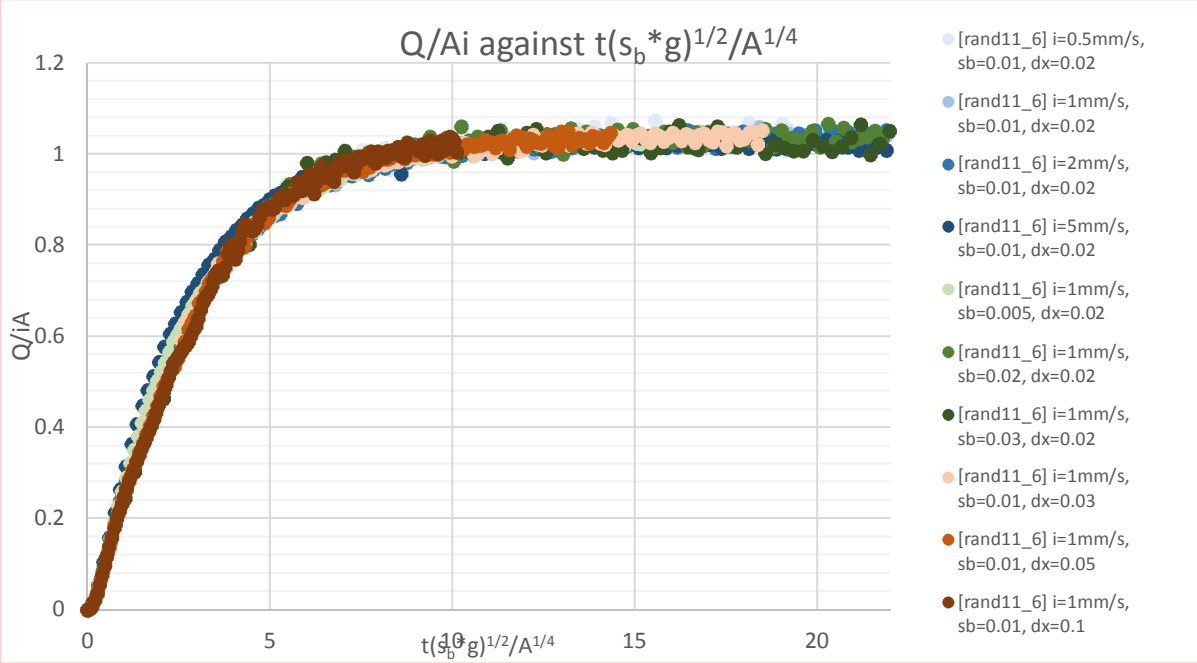

Figure 11 Dimensionless Flow against Dimensionless Time (Verification, random matrix)

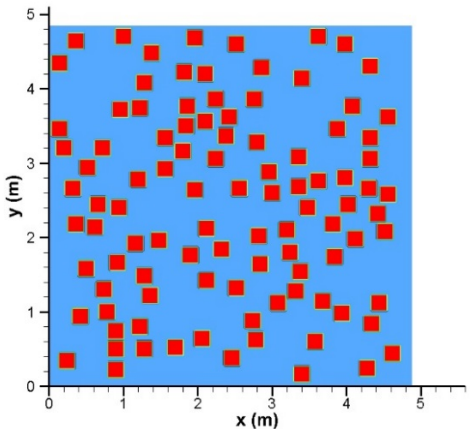

Figure 12 Random configuration used in verification test 2

Model Application

The model was applied to investigate effects of buildings and bed roughness to the time of concentration. Before the investigations, in section 1 it was confirmed that the choice of resolution and catchment would not affect the results. This paved the foundation for sections 2, 3 and 4 to show impacts of varying building area ratio (BA), building density and bed roughness.

1. Choice of Resolution and Catchment

1.1 Choice of resolution

Twelve 1x resolution and Twelve 2x resolution simulations were done with random buildings, each using i=1mm/s, s_b=0.01 and A=23.474 m^2 (equivalent to Δx=0.02m (1x resolution)/0.01m (2x resolution)). Building area ratio and density remained the same throughout: BA=24.5%, 100 buildings. A t-test was done with the 24 samples, as shown in Table 1. With a t stat of 0.3907 in 95% confidence level, using a two-tail test, it could be concluded that regardless of using 1x or 2x resolution, times of concentration were statistically indifferent.

	2x Resolution	1x Resolution
Mean	3.15832003	3.19420731
Variance	0.05784937	0.043382486
Observations	12	12
Pooled Variance	0.05061593	
Hypothesized Mean Difference	0	
df	22	
t Stat	-0.3907262	
P(T<=t) two-tail	0.69975762	
t Critical two-tail	2.07387307	

Table 1 t-Test of 1x and 2x resolution test assuming equal variances, Random Samples

Comparisons of results from 1x resolution and 2x resolution were also done on regular matrices. Topographic and hydrological conditions were maintained as above. Building area ratio was kept at 24.5% but building density was varied. The influence of sizes due to resolution could then be observed. This was more feasible with regular matrices because there could only be one configuration for one number of buildings.

With 25 (5x5), 36 (6x6), 64 (8x8), 100 (10x10), 144 (12x12) and 225 (15x15) buildings simulated, graph of dimensionless flow versus dimensionless time was obtained and t-tests with pair samples were completed with the dimensionless t_{70} results. The graph in Figure 13 showed that most building configurations in both 1x resolution and 2x resolution generally collapsed onto an S-curve, with the exception of 225 buildings in 1x resolution. Results from Table 2 showed that at 95% confidence level, there was insufficient evidence to show that using 1x resolution would cause statistically different t_{70}. Therefore, it could be safely assumed that mean dimensionless t_{70} from 1x or 2x resolution would be the same.

If samples of 225 buildings were excluded however, it could be shown that variance of data set was decreased and the P-value was increased. This exclusion was based on the fact that having 225 buildings in 1x resolution would lead to each building having a side length of 8 grid points. Therefore, the t_{70} obtained from this sample significantly deviated from the rest simulations. Result after exclusion could be seen in Table 3. It could be shown that the P-value actually increased from 0.179 to 0.247, conforming our inspection. This indicated that buildings with small side length may cause significant error in capturing the flow.

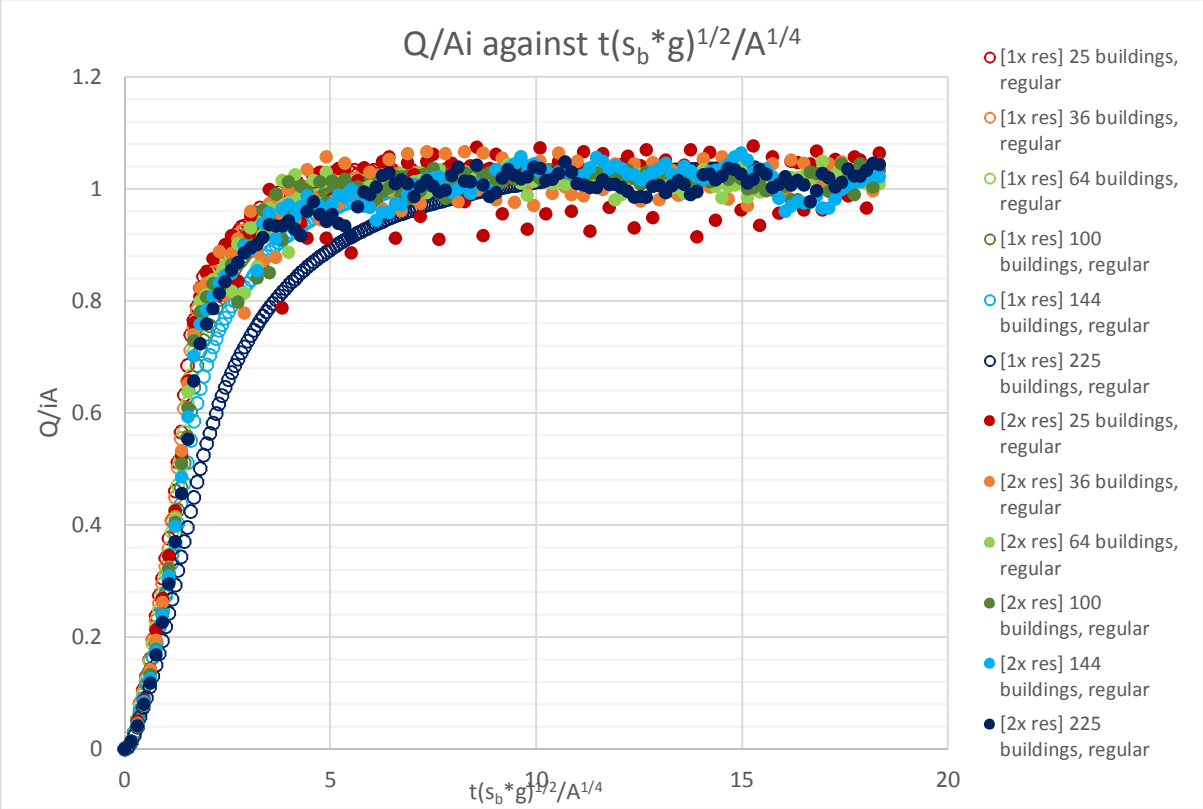

Figure 13 Dimensionless flow against Dimensionless time, Regular Buildings, Varied Building Density

	2x resolution	*1x resolution*
Mean dimensionless t_{70}	1.654041	1.908362
Variance	0.004479	0.216186
Observations	6	6
Hypothesized Mean Difference	0	
df	5	
t Stat	-1.562974	
P(T<=t) two-tail	0.178821	
t Critical two-tail	2.570582	

Table 2 t-Test: Paired Two Sample for Means (including 225 buildings (side length 8)

	2x Resolution	*1x Resolution*
Mean dimensionless t_{70}	1.629557	1.733803
Variance	0.001102	0.041703
Observations	5	5
Hypothesized Mean Difference	0	
df	4	
t Stat	-1.353605	
P(T<=t) two-tail	0.247295	
t Critical two-tail	2.776445	

Table 3 t-Test: Paired Two Sample for Means (225 buildings excluded)

In view of this difference, 2x resolution was used in all other parts of investigation. This was to ensure that even in high building densities or low building area ratio, the side length would still be above 10 grid points. The importance of having side length above 10 grid points (irrespective to Δx) was that resolution may not be high enough to capture reverse flow at the end of each building. This would cause overestimation of time of concentration.

1.2 Choice of catchment

Tests were done with the same building density, grid size, rainfall and bed gradient (Δx=0.01 m, i=1 mm/s, s_b=0.01), but one group with twice the catchment side length of the other group, hence double the number of buildings in each dimension. Different regular building patterns were used and were shown in Figure 14:

3x3, 4x4, 5x5, 6x6, 8x8 and 10x10 buildings in small catchment (A=2.43x2.43 m=5.9049m^2)

6x6, 8x8, 10x10, 12x12, 16x16, 20x20 buildings in big catchment. (A=4.86x4.86 m= 23.6196m^2)

T-test with paired samples was done to compare t_{70} of simulations, as shown in. Results showed that there was insufficient evidence to show that times of concentration of big catchment varied with results of small catchment. This may suggest that the choice of catchment made little influence to the analysis result. Choosing a small local area in analysis would give similar results to choosing a larger area, providing if building area ratio and density remain unchanged.

3x3 (small)
6x6 (big)

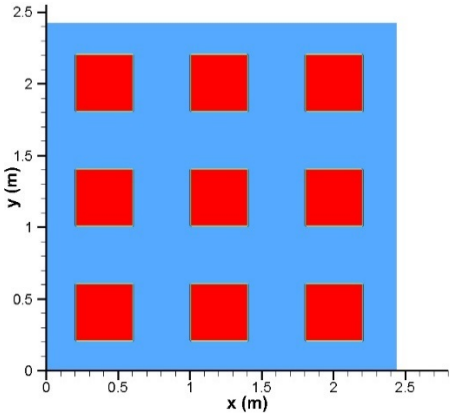

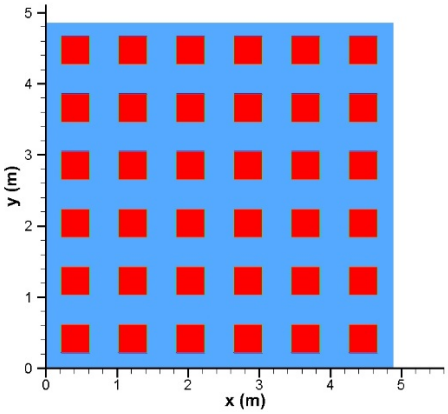

4x4 (small)
8x8 (big)

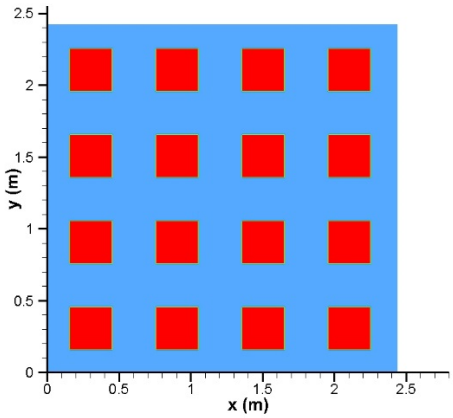

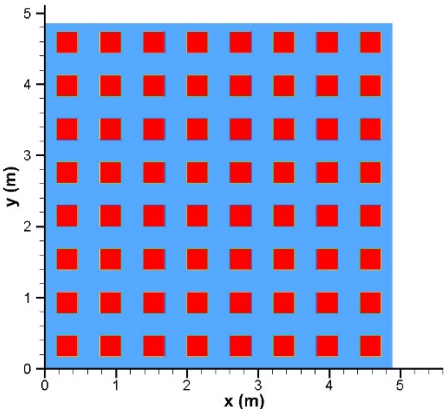

5x5 (small)
10x10
(big)

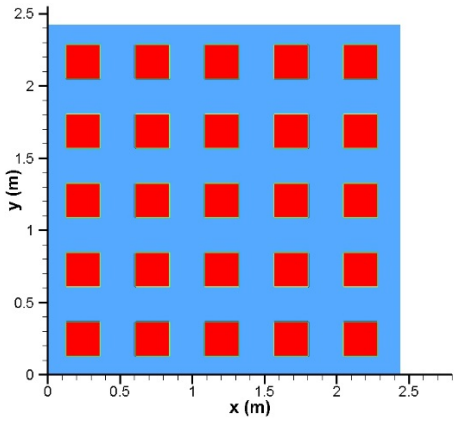

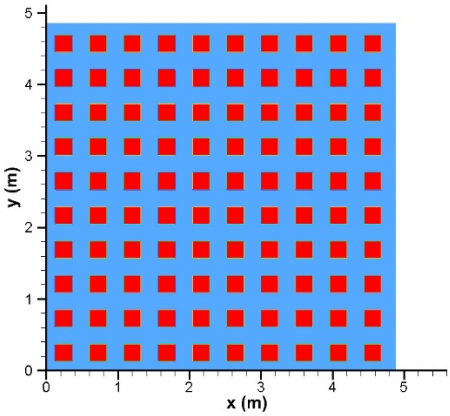

6x6 (small)

12x12

(big)

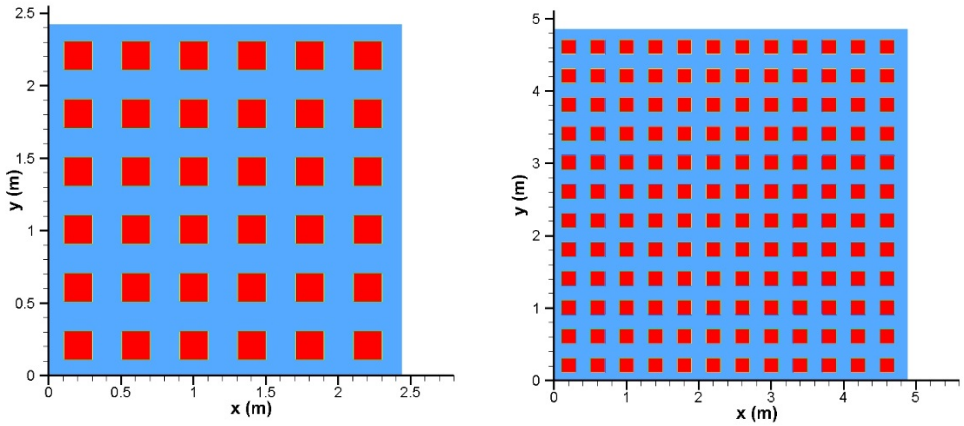

8x8 (small)

16x16

(big)

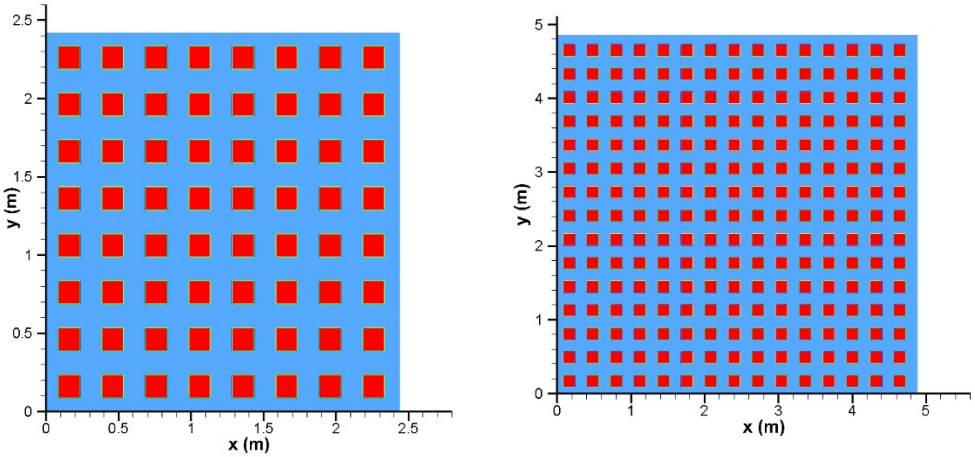

10x10

(small)

20x20

(big)

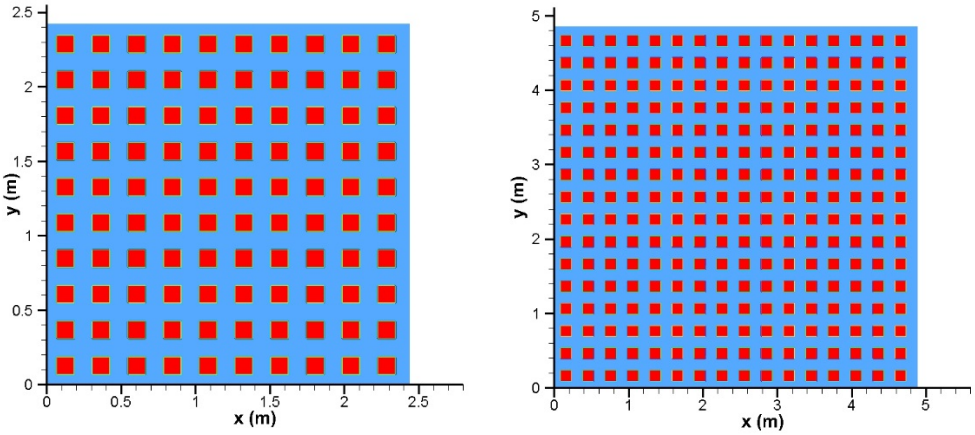

Figure 14 Building configurations in verification test 4

	Big Catchment	*Small Catchment*
Mean	1.738316	1.710746
Variance	0.030432	0.017292
Observations	6	6
Hypothesized Mean Difference	0	
df	5	
t Stat	1.461187	
P(T<=t) two-tail	0.203805	
t Critical two-tail	2.570582	

Table 4 t-Test: Paired Samples of big and small catchment

In the following investigations, the same hydrological and topographic conditions were used. i=1 mm/s, s_b=0.01 and A=23.474 m^2 (Δx=0.01 m (2x resolution)). Regular, staggered and random building patterns would be tested. As demonstrated in verification, when these parameters were changed in real situations, the dimensionless term of time and flow would be able to capture the change. 2x resolution was used throughout to ensure a minimum building side length of 10 grid points in computation.

2. Influence of Building Area Ratio

2.1 Studied Cases

Simulations were done with fixed catchment size, building density and Chezy coefficient $C = 1 \times 10^{30}\ m^{\frac{1}{2}}s^{-1}$. Building area ratio (BA) and building pattern were varied. 2 sets of simulations were done: one with 100 buildings and another with 64 buildings.

For each set of simulations, tests were done with 5%, 10%, 20% and 30% of catchment area for all building patterns, plus 15% and 25% for staggered matrices only. The unique configuration of regular and staggered pattern will be used for each of the BA. For random pattern, 4 configurations would be tested at BA=5% and 10%; 7 configurations for BA=20% and 30% for both 64 and 100 buildings. Figure 15 showed configurations used in BA=30%, 64 buildings. Beyond 30%, the terrain would be very congested and flows would be severely affected by how buildings were exactly arranged. Water may even fail to reach the end of catchment. This defied the purpose and execution of project, which aimed to find a general relationship between times of concentration and other parameters.

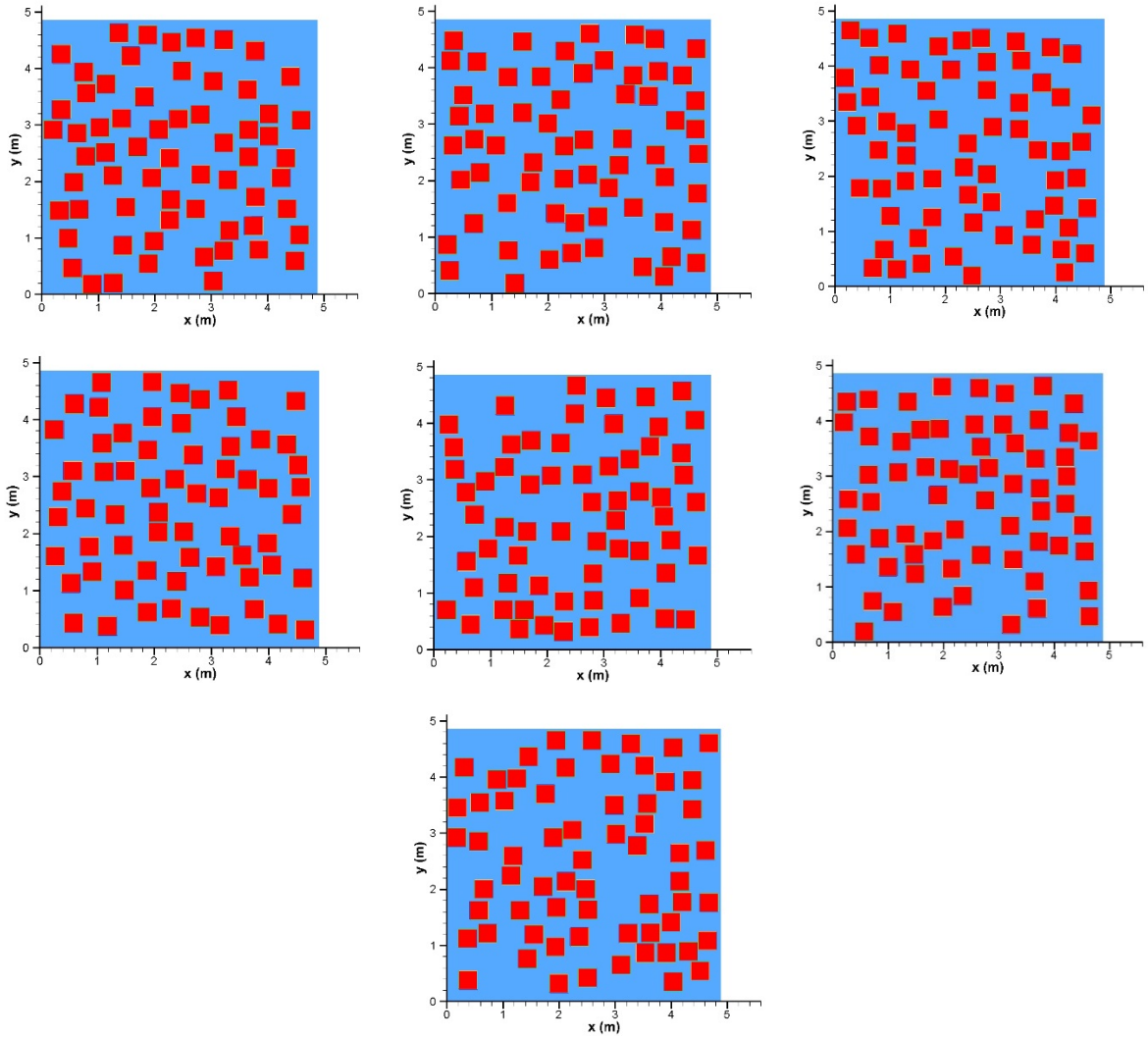

Figure 15 Configurations of BA=30%, 64 buildings

2.2 Non-dimensional S-curve and Time of concentration

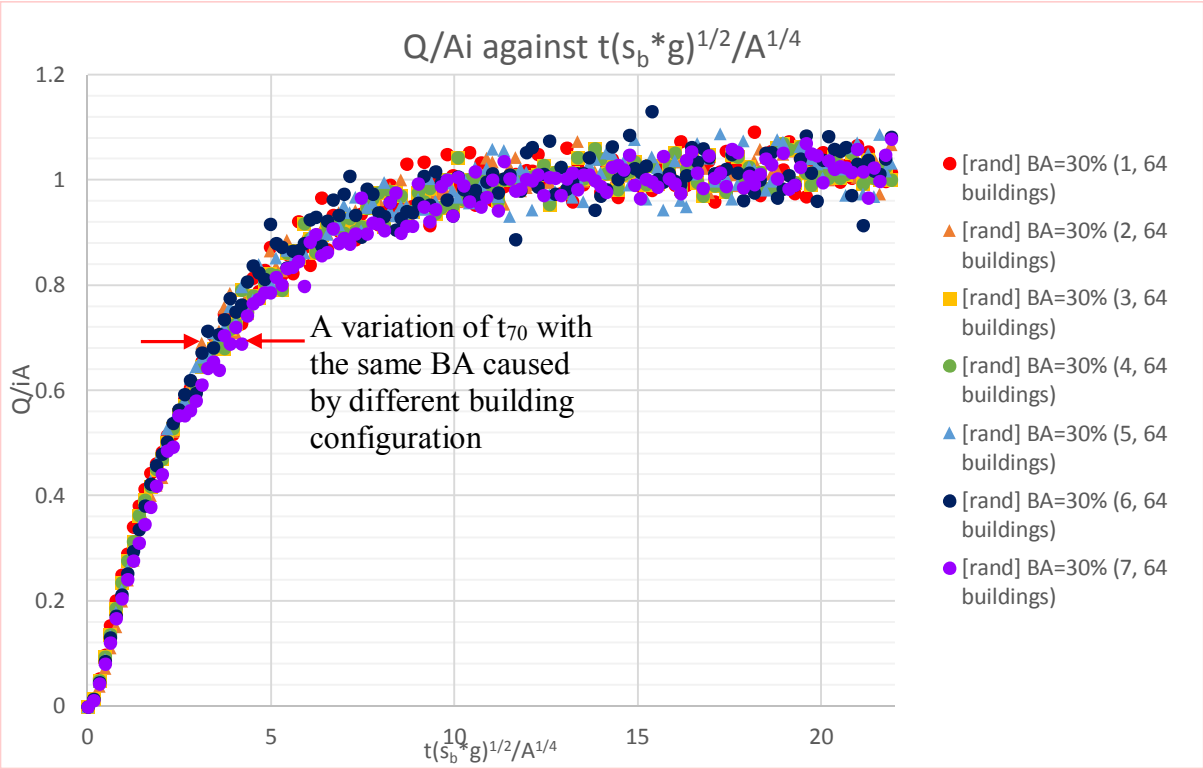

Figure 16 Dimension flow against dimensionless time, BA=30%, 64 buildings

Graphs were plotted with dimensionless flow and time. With the same BA and same building density, there would only be one curve for regular and staggered matrix, because there was only 1 configuration that satisfied both the BA and building density. For random matrices, a series of curves could be plotted because multiple random configurations were permitted. Figure 16 showed the 7 dimensionless flow curves obtained from the 7 catchment configurations shown in Figure 15. There would be a variation of t_{70} results, as indicated in Figure 16. This variation was captured by calculating the mean of results and specifying the maximum and minimum values obtained. From tests of different BA and building pattern, graphs of dimensionless time of concentration versus BA were plotted, as shown in Figure 17 and Figure 18.

Referring to results in Figure 17 and Figure 18, in general, time of concentration increased with increasing building area ratio. The simplest relationship was used for lines of best fit, wherever the R-squared value reached 0.9 or above. Error bars on data points of random matrices indicate the maximum and minimum value obtained with the specific BA.

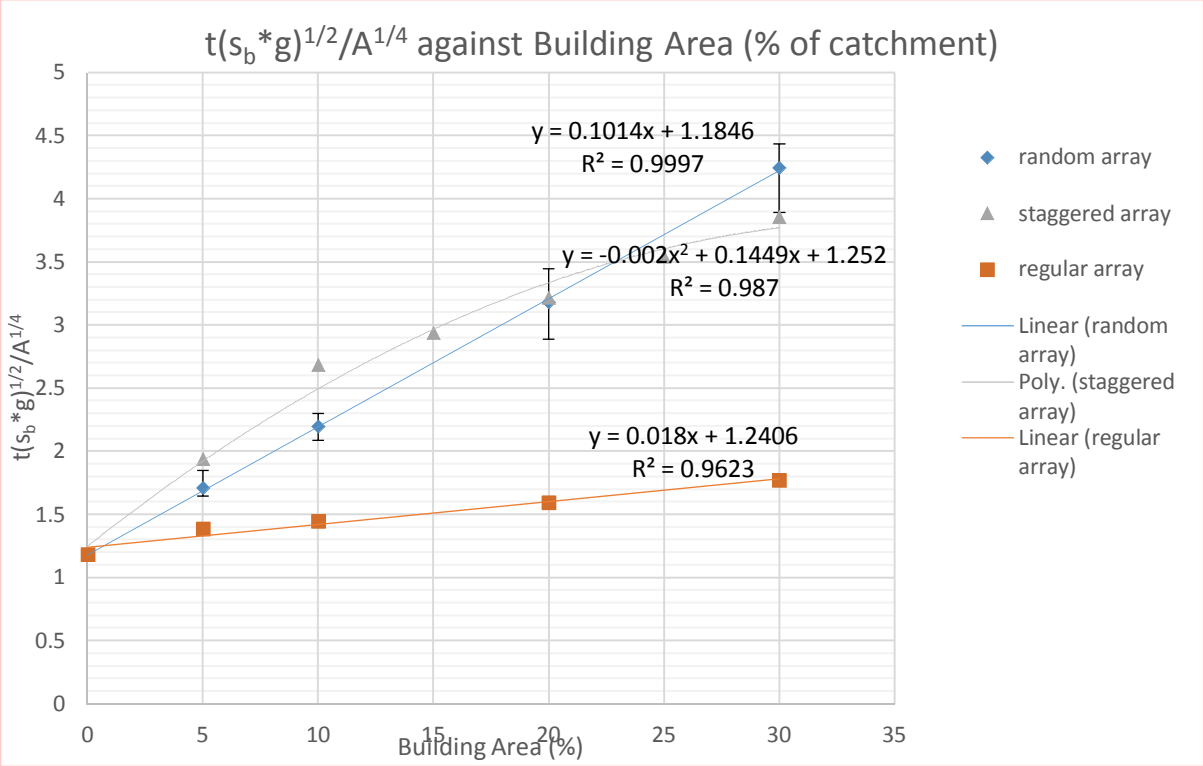

Figure 17 Relationship of Dimensionless t_{70} versus Building Area Ratio (100 Buildings)

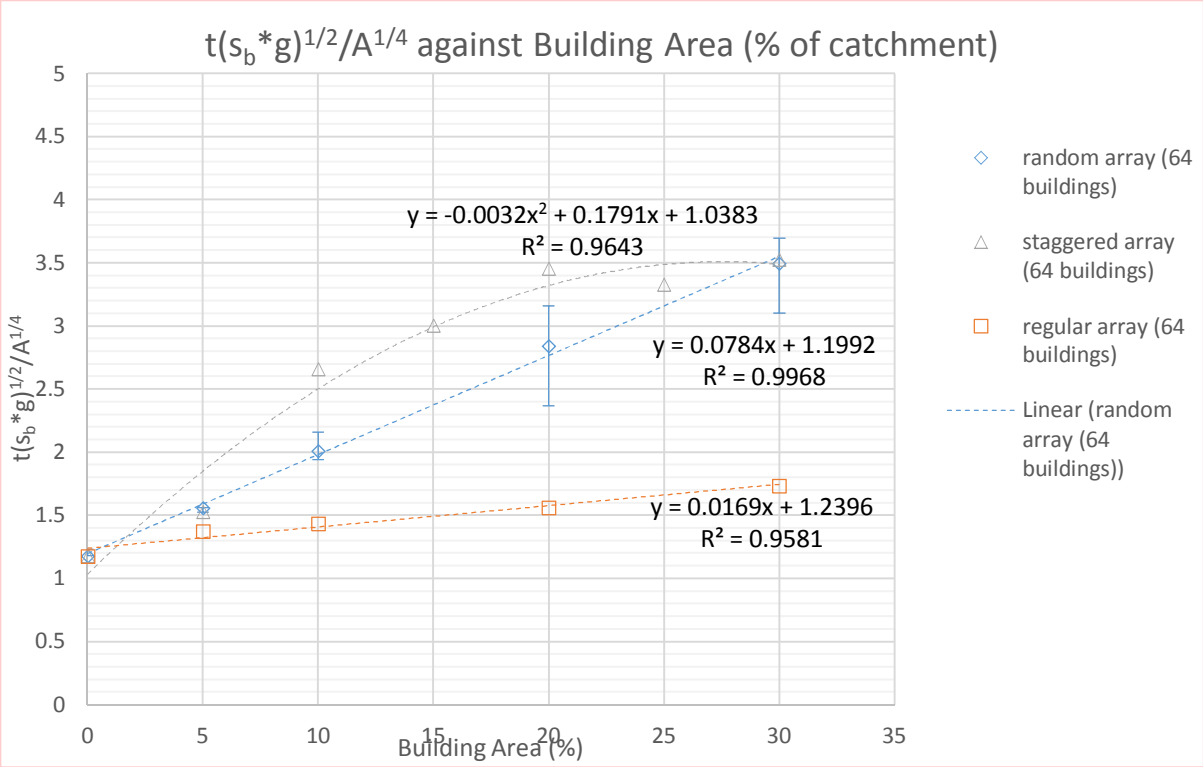

Figure 18 Relationship of Dimensionless t_{70} versus Building Area Ratio (64 Buildings)

The trend relationship however varied between building patterns.

Regular: Time of concentration increased with increasing building area ratio linearly. Gradient of the line of best fit was much lower than that of other patterns, indicating that the change of time of concentration with building area ratio was not as significant as random matrices. Trends of 64 buildings and 100 buildings were very similar, agreeing with results from building density investigation. This suggested that for regular matrices, building density played little role in affecting times of concentration but building area ratio made more impacts.

Random: Time of concentration increased with increasing building area ratio linearly. For both 64 buildings and 100 buildings, linear lines fitted onto their data well, as the R-square reached 0.996 or above. As shown in the graphs, with bigger building area ratio, difference caused by building density became more pronounced. Results also suggested that specimens from higher building area ratio gave a higher variation, although standard deviations were less than 10% of mean in all situations.

Staggered: Time of concentration increased with building area ratio in a parabolic relationship. A high R-square value could only be obtained with parabolic curves because the rise of t_{70} was steeper in low BA than in high BA. Curves for 64 buildings and 100 buildings were similar to each other. Noted that because of having a negative second order term in the quadratic equation, the equations could only be used up to BA=30%. It was not realistic to have a lower t_{70} with even higher BA.

2.3 Flow Field Examination

As demonstrated by results in the previous section, increasing building area ratio resulted in increased time of concentration. Effect of buildings could be explained by the following concept.

2.3.1 Explanation of increasing t_c with increasing BA

Although viscosity effect ($\frac{dV}{dz}\ term$) was neglected in shallow water equation, flow rate still changed because of obstructions in domain. Q_x was the parameter measured and $Q = \sum(A_x \cdot v)$. A_x was the cross-sectional area of flow across the plane at certain distance in x-direction; v was the velocity of flow.

Inserting buildings in the terrain would make water flow more convoluted, hence increasing the drainage path and reducing the speed v. If bed roughness was introduced (to be introduced in section 4 of *Model Application*), the increased length would lead to more frictional effect and further reduce the flow speed.

Also, when water hit the front of buildings, it would transfer its kinetic energy into potential energy, i.e. water accumulated and water depth rose. Water was also diverted to flow around the building, creating a boundary that slowed down the dominant flow. At the end of buildings, some reverse flows were observed when flows from either side of building merge into a stream. These kinetic energy losing actions were summarized in Figure 19. Hence, velocity v was reduced.

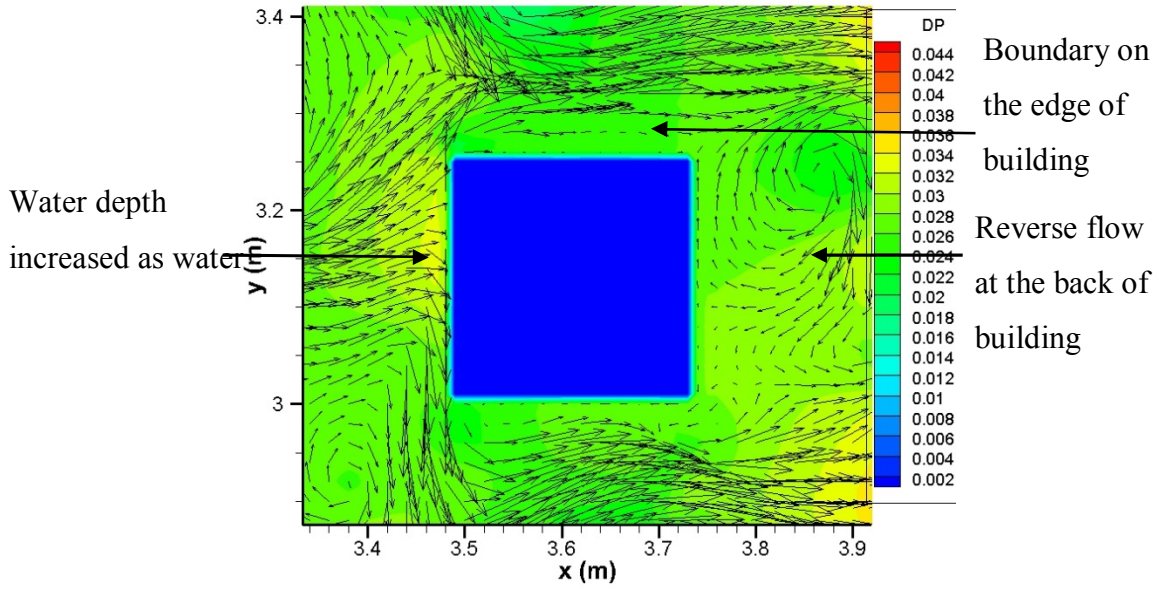

Figure 19 Flow at a building (BA 25%, 100 buildings, staggered)

Therefore, a plain terrain without buildings reached its maximum flow Q_x the fastest and had the lowest time of concentration. A terrain with higher building area ratio would result in lower Q_x and longer time of concentration.

It was previously thought that building area ratio was the only influence of buildings exerted to the flow but results showed the contrary. When the building area ratio was held constant, the cross sectional area A_x remained the same. Analogies could be made between this flooding analysis and pipeline networks. 5 big pipes should yield a similar cross sectional area as 10 small pipes. Hence it was previously thought that as long as the building pattern was fixed, cross sectional area across planes along the direction of flow would be held constant, leading to the same flow pattern and same time of concentration.

The contrary to the hypothesis above was shown. In Figure 20 to Figure 25, it could be seen that flow patterns between buildings were not identical as BA increased from 5% to 30%. All channel flow shots were captured at t=15 seconds of simulation. The channel that flowed at maximum flow rate was narrower at high BA. Therefore, building patterns may

change the flow. This overthrew the hypothesis of same cross sectional area and led to the investigation of building density as shown in section 3.

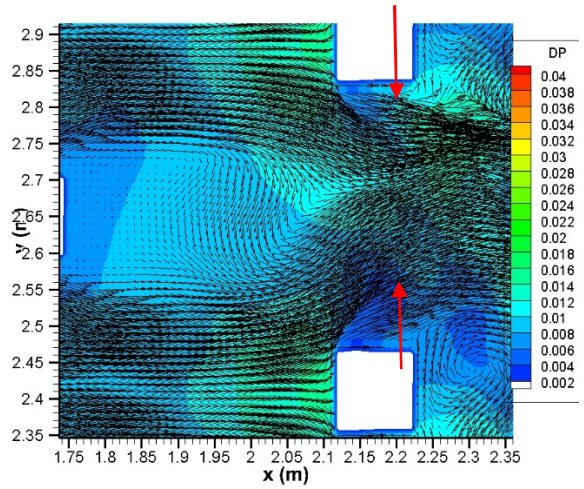

Figure 20 Close view (BA=5%)

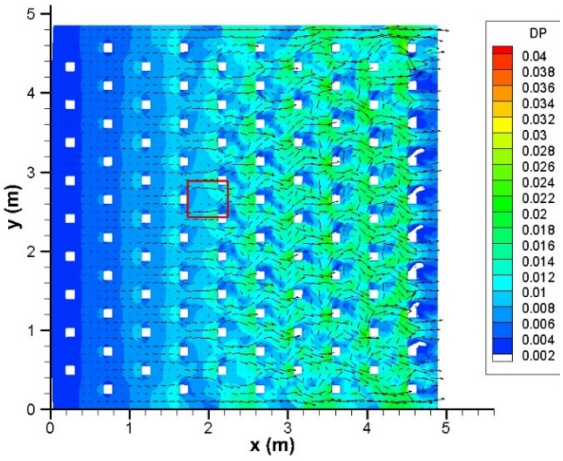

Figure 21 Overview (BA=5%)

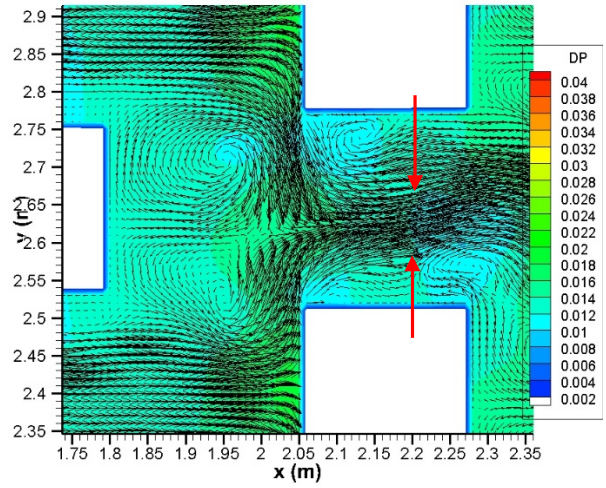

Figure 22 Close View (BA=20%)

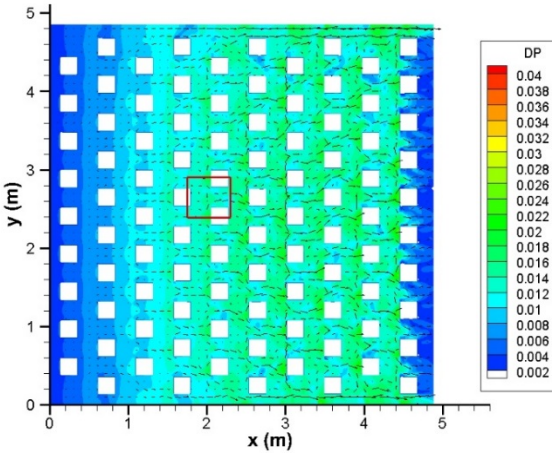

Figure 23 Overview (BA=20%)

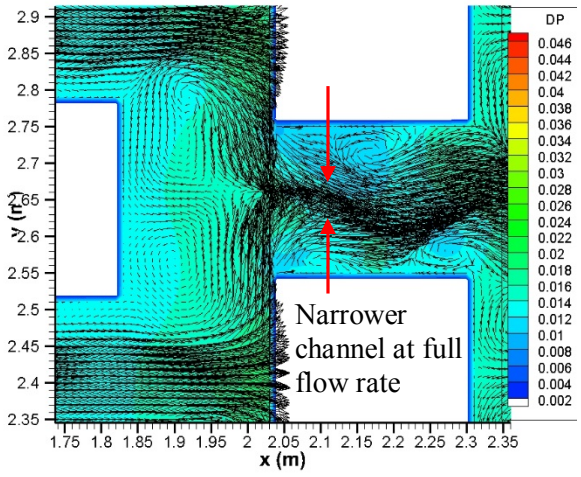

Figure 24 Close View (BA=30%)

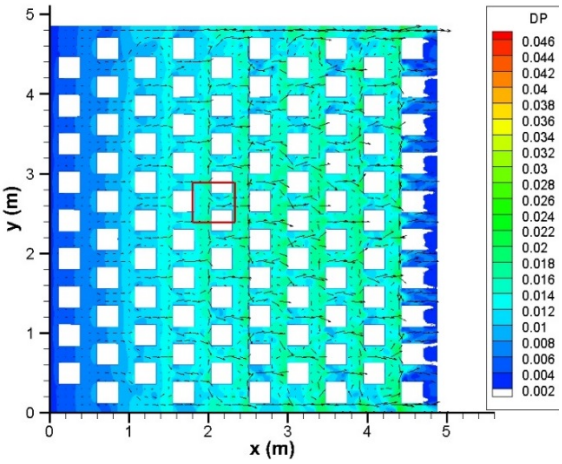

Figure 25 Overview (BA=30%)

2.3.2 Explanation of staggered t_c crossing random t_c

In Figure 17 and Figure 18, it was demonstrated that time of concentration recorded by staggered matrices was higher than that recorded by random matrices in low BA, but the reverse happened in high BA. This phenomenon could be appreciated in flow field diagrams in Figure 26. All diagrams were captured in t=80s (when flow had already saturated) and all scenarios contained 100 (or for staggered, nearest to 100) buildings.

Comparing flow fields of staggered and random matrices in BA=10%, it could be seen that there were relatively large spaces in random matrix configuration. A few buildings may cluster in a certain region as a result of randomization. This clustering resulted in little convolution and little energy dissipation in buildings. As the figure of random matrix at BA=10% illustrated, on left hand side of domain flow paths were relatively straight. In contrast, in staggered matrix, positions of buildings were fixed, hence the flow path was pre-determined to be convoluted in a certain pattern. Weighing the amount of convolution and dissipation, it was possible for flow in staggered matrix to have more. Therefore, t_c in staggered matrix was higher than that in random matrix.

Comparison in BA=30% would however arrive in an opposite conclusion. Even though the number of buildings were the same (100 throughout), because of bigger buildings required, convolution and subsequent dissipation were evident in the random matrix scenario. Open plains and parallel flow paths happened much less than in BA=10%. In staggered building matrix, even when buildings had enlarged in BA=30%, positions of buildings remained the same. The extra convolution only came from enlarged buildings. Therefore, it was possible to have fewer convolutions and energy dissipation in staggered building matrix than in random matrix, hence lower time of concentration.

Regular matrices were shown here for reference. It could be seen that open straight channels were present at both BA=10% and BA=30%. Few convolutions existed. Therefore, the times of concentration and the increase with building area ratio were lower than both staggered and random matrices.

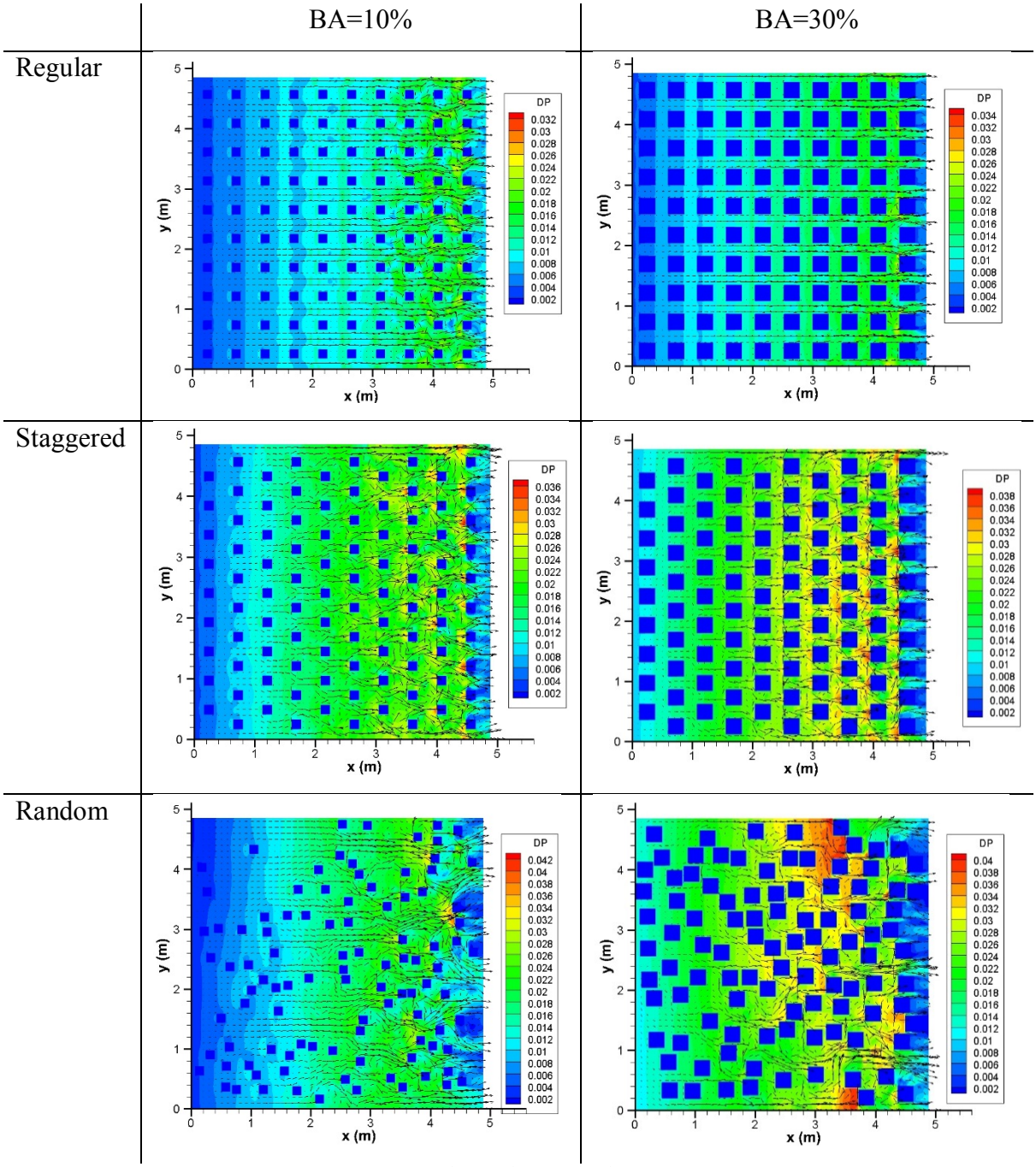

Figure 26 Flow and water depth at t=80s

3. Influence of Building Density

3.1 Studied Cases

Keeping hydrological and topographic condition fixed as above, simulations were done with identical Chezy coefficient $C = 1 \times 10^{30}\ m^{\frac{1}{2}}s^{-1}$ and building area ratio (24.5%). The varying parameters were the building density and building pattern. Number of buildings tested were: 25, 36, 64, 100, 144, 225 and 400. Building configurations were unique in

regular and staggered pattern so 1 combination was tested with each of the number of buildings; 4 random pattern configurations were tested for each number of building.

It was previously thought that building density would not affect the time of concentration because different building patterns should have already captured the influence of number of buildings. This hypothesis was overthrown by this set of simulation results because the times of concentration were shown to vary with building density. This may not be significant in regular patterns, but was certainly evident in staggered and random building matrices.

3.2 Time of Concentration Graphs

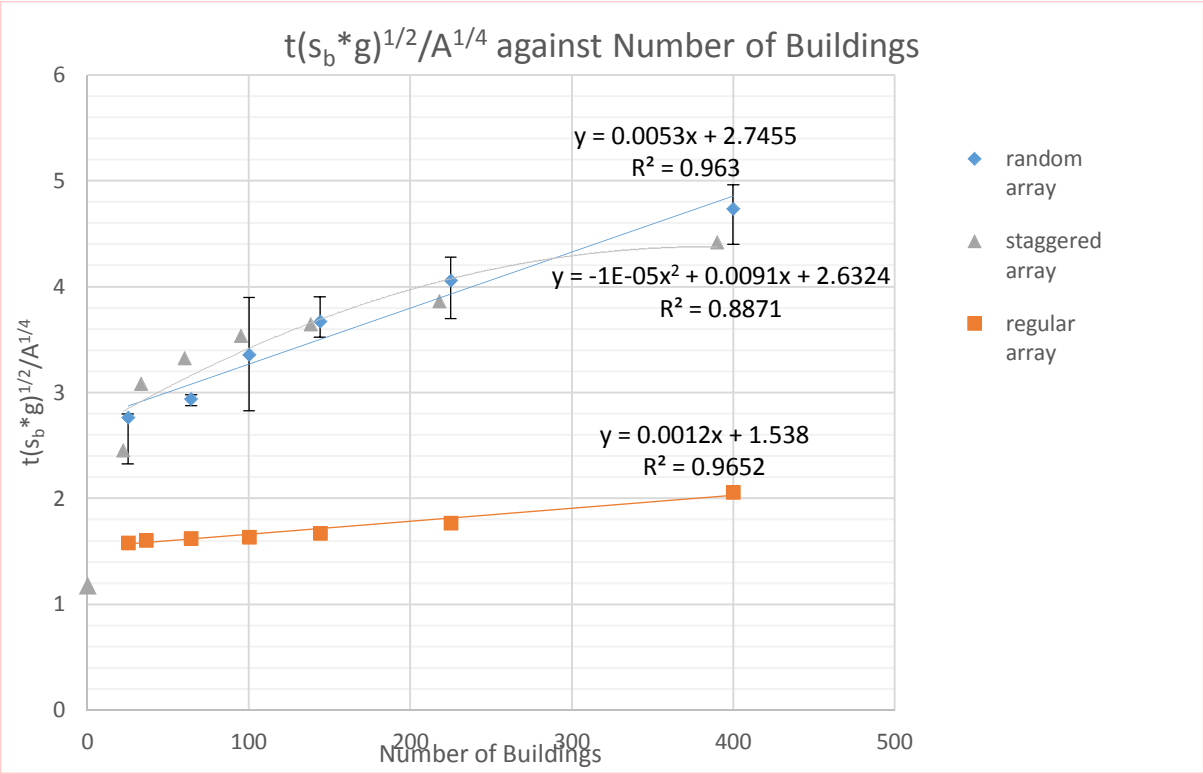

Figure 27 Relationship of dimensionless t_{70} versus the number of buildings

With reference to Figure 27, time of concentration generally increased with building density. Same as the investigation of building area ratio, relationship of the increases differed between building patterns. Error bars above and below data points of random array tests indicated the maximum and minimum t_{70} obtained in the same number of buildings.

Regular: time of concentration increased with building density linearly. The high R-square value of 0.9652 suggested that the linear relationship between times of concentration and building density was significant.

Random: time of concentration increased with building density linearly. The high R-square value of 0.963 suggested that the linear relationship between times of concentration and building density was significant.

Staggered: time of concentration increased with building density. The effect was more prominent in small number of buildings, but the rise levelled off with more than 100 buildings in catchment, hence a parabolic curve gave better correlation. Although the R-square value was below but close to 0.9, quadratic relationship was the most sensible relationship found to approximate the relationship. Beyond the second order, unphysical rise and fall of time of concentration would be caused.

3.3 Flow Field Examination

3.3.1 Explanation of increasing t_c with building density

As illustrated in section 3.2, time of concentration increased with increasing number of buildings. The increase was found linear in regular or random pattern but quadratic in staggered pattern.

Building density affected the time of concentration by having water to flow at varying rate across a channel. Simulations shown in Figure 28 and Figure 29 were done with the same hydrological and topographic conditions. The only difference between them was the number of buildings in catchment (Figure 28 with 217 buildings, Figure 29 with 22 buildings, all in staggered pattern). Arrows indicated unit width flow in the grid, all with the same spacing and magnification. As shown in Figure 28, the separation layer that had slower flow occupied 2 grid points of width along each edge. In Figure 29, the layer was 3 grid points wide. The channel size shown in Figure 29 was in comparison much bigger than the channel in Figure 28. Therefore, this indicated that the channel was more utilized in small number of buildings than large ones. Hence in scenarios with fewer buildings, flows were faster and the time of concentration was lower.

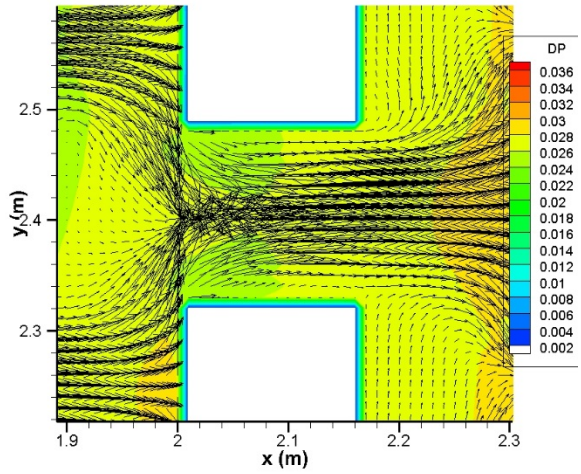

Figure 28 Flow between buildings (217 buildings, BA 24.5%, staggered)

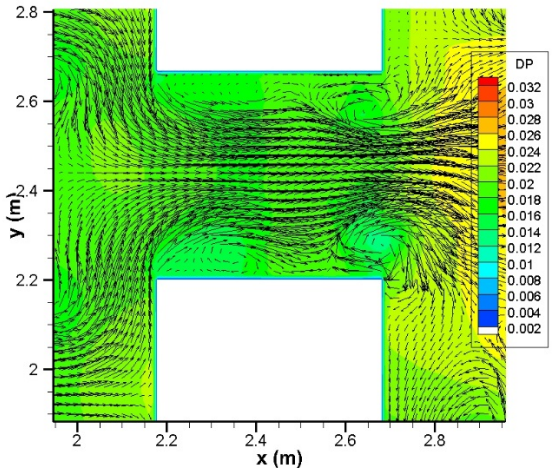

Figure 29 Flow between buildings (22 buildings, BA 24.5%, staggered)

3.3.2 Explanation of staggered t_c crossing random t_c

In Figure 27 it was demonstrated that t_c of staggered matrices was higher than that of random matrices in low building density, but the pattern was reversed in high building density. This phenomenon could be appreciated in flow field and velocity field diagrams in Figure 30. Scenarios with 100 and 400 buildings were chosen to illustrate the crossing. All diagrams were captured in t=100s (when flow had already saturated) and the same magnification applied on arrowheads.

Comparing flow fields of staggered and random matrices with 100 buildings, it could be seen that there was relatively large space in random matrix configuration. A close examination of velocity fields also revealed that flows in a larger proportion of channel was flowing at high velocity in random matrix. As explained in section 3.3.1, a better utilization of channel would bring the t_c down. Therefore, t_c in staggered matrix was higher than that in random matrix.

Comparison of 400 buildings scenarios would however arrive in an opposite conclusion. Because of increased building density, the free space found in 100 building random matrix appeared much less frequently. Buildings were now more scattered due to randomized allocation of position. Separation layer could now be developed across multiple small buildings, causing a much lowered channel utilization. In contrast, because of fixed meandering pattern, in staggered matrix channel utilization did not drop as much. Therefore, staggered matrix would have higher velocity than random matrix in 400 buildings scenario, hence a lower time of concentration.

	100 Buildings	400 Buildings
Staggered Flow Field	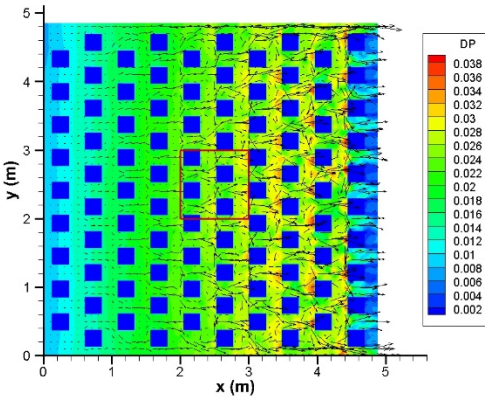	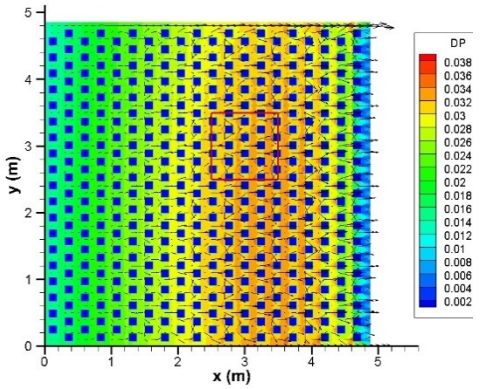
Staggered Velocity Field	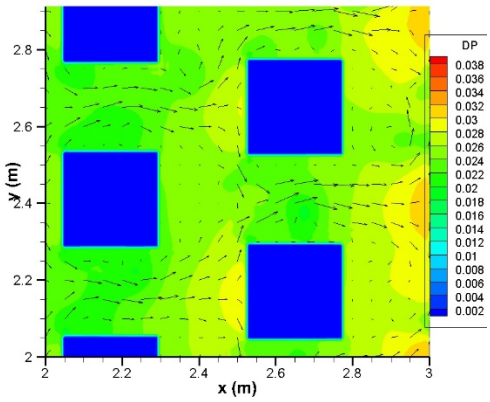	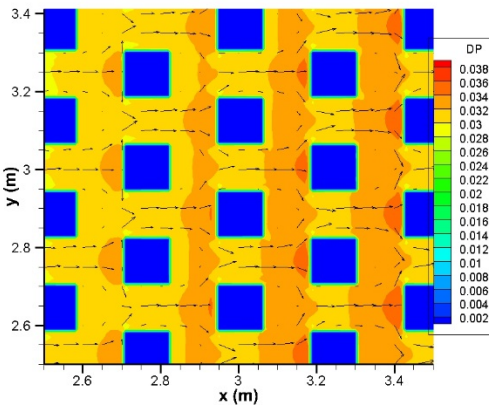
Random Flow Field	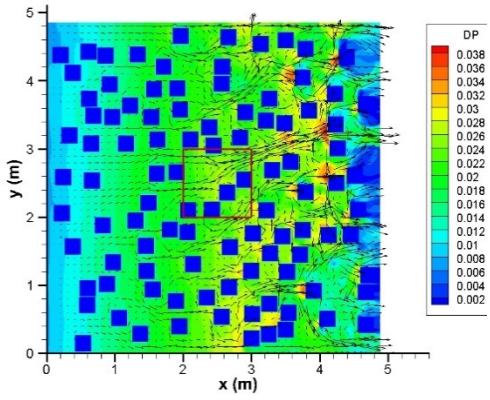	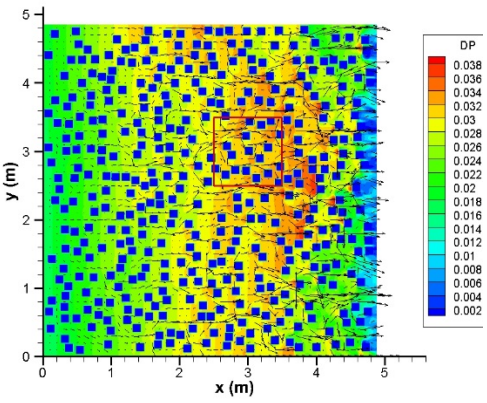
Random Velocity Field	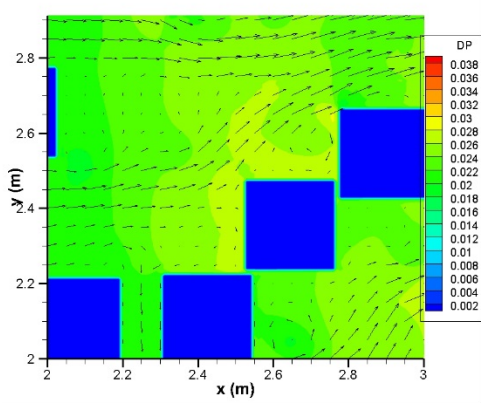	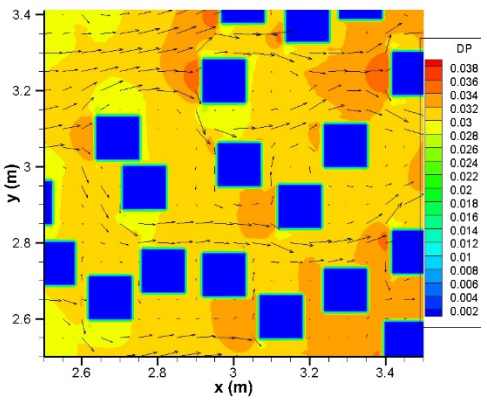

Figure 30 Flow fields and Velocity fields at t=100s, staggered and random matrices

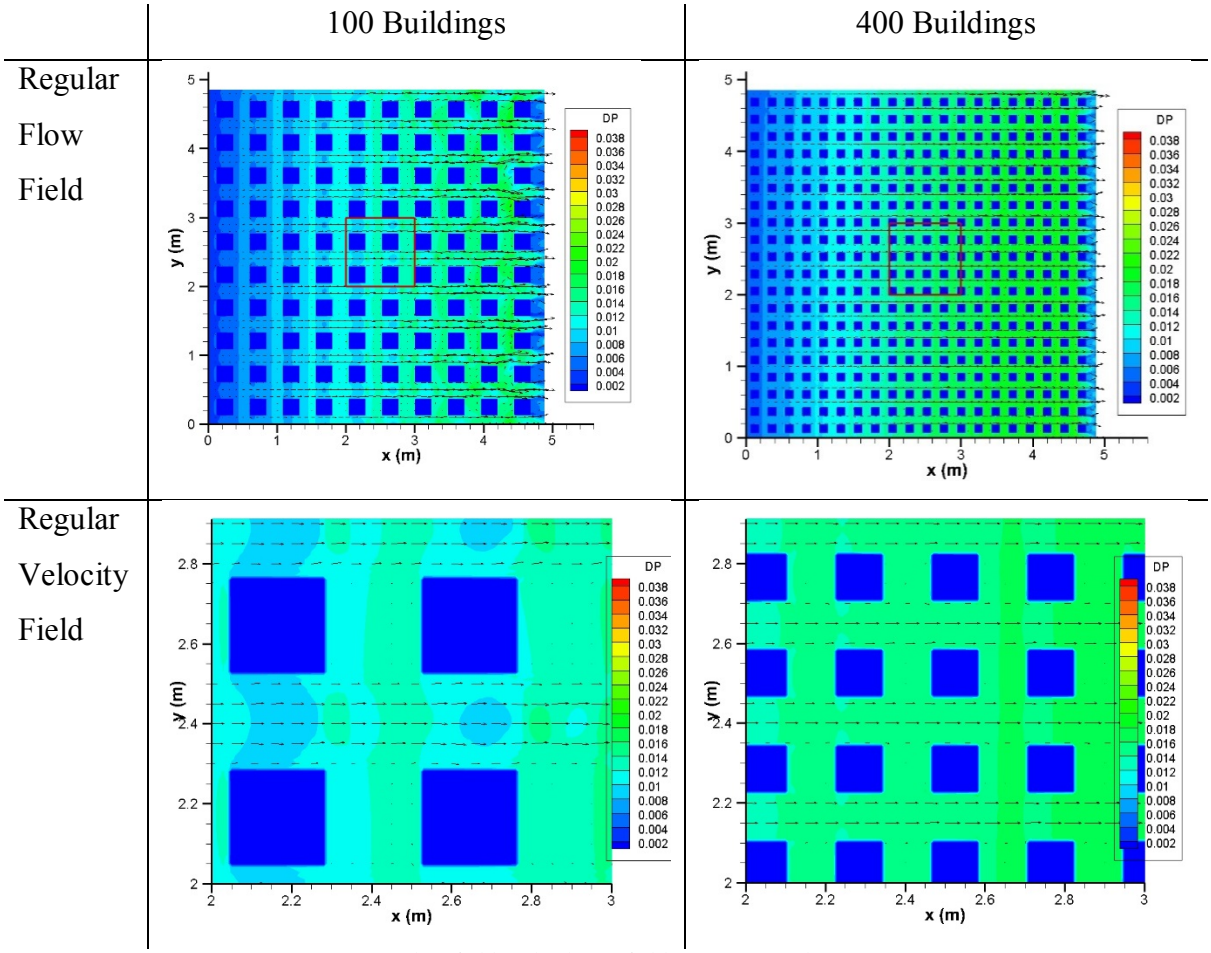

Figure 31 Flow field and velocity field, t=100s, regular matrices

Regular matrices were shown in Figure 31 for reference. It could be seen that open straight channels were present at both 100 and 400 buildings. Most water flowed in the straight channels. Therefore, the times of concentration was lower than both staggered and random matrices.

4. Influence of Bed Roughness

4.1 Studied Cases

Keeping hydrological and topographic condition fixed as above, simulations were conducted with identical building area ratio (24.5%) and number of buildings (100). The varying parameters were the bed roughness and building pattern. Two methods declaring bed roughness were tested; computation was conducted with bed roughness height (k_s) and manning's coefficient (n) respectively. One configuration of regular, staggered and random pattern was tested. The random pattern configuration used was shown in Figure 32.

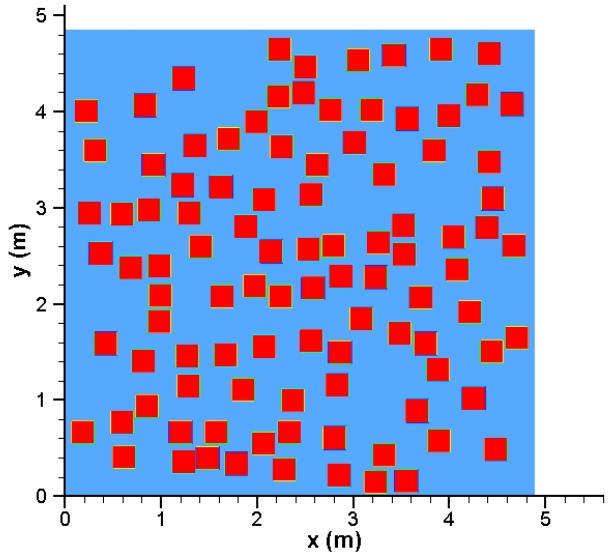

Figure 32 Random pattern configuration used in Bed Roughness tests

4.2 Non-dimensional S-curve and Time of Concentration

With reference to Figure 33, it could be shown that time of concentration increased with bed roughness in linear relationship for all building patterns. All regression lines were drawn with R-square values above 0.95, indicating that the linear relationship between bed friction and dimensionless times of concentration was very strong. In real life situations, $n = 0.01m^{\frac{-1}{3}}s$ to $n = 0.05m^{\frac{-1}{3}}s$ should have included friction values of common materials so the range examined could be relied on with confidence.

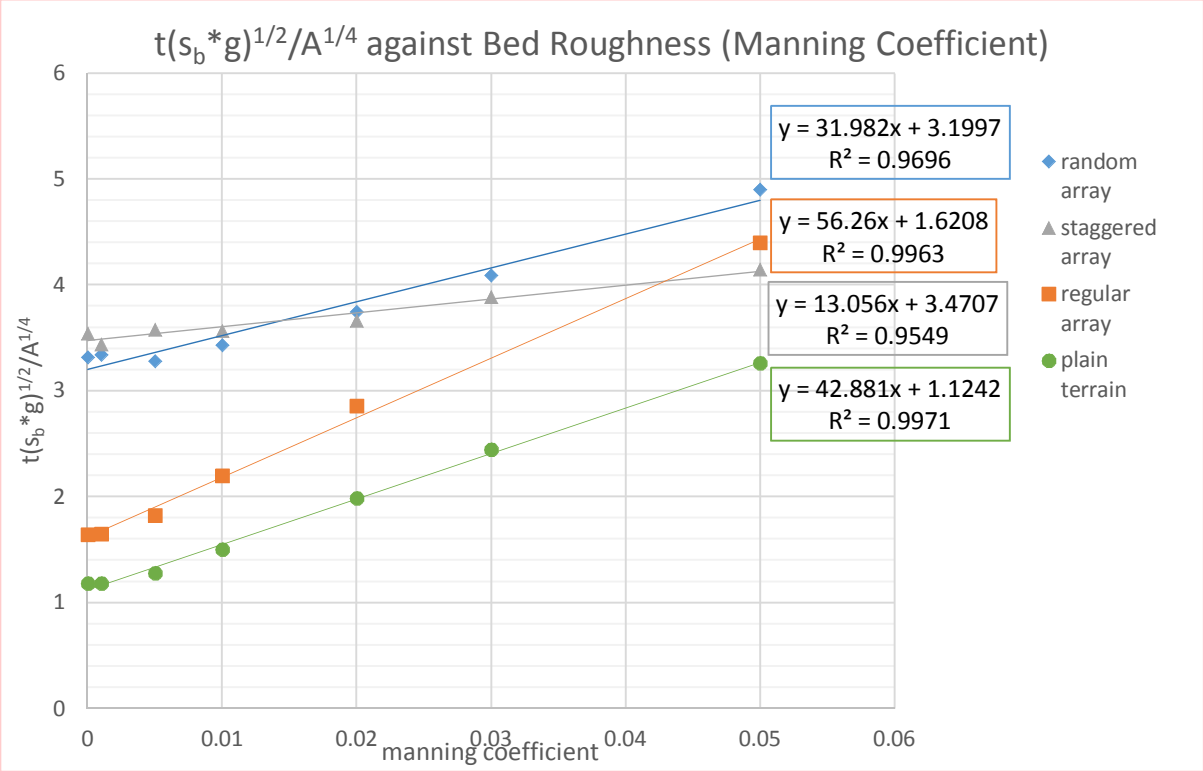

Figure 33 Relationship of dimensionless t70 versus Bed Roughness (manning coefficient)

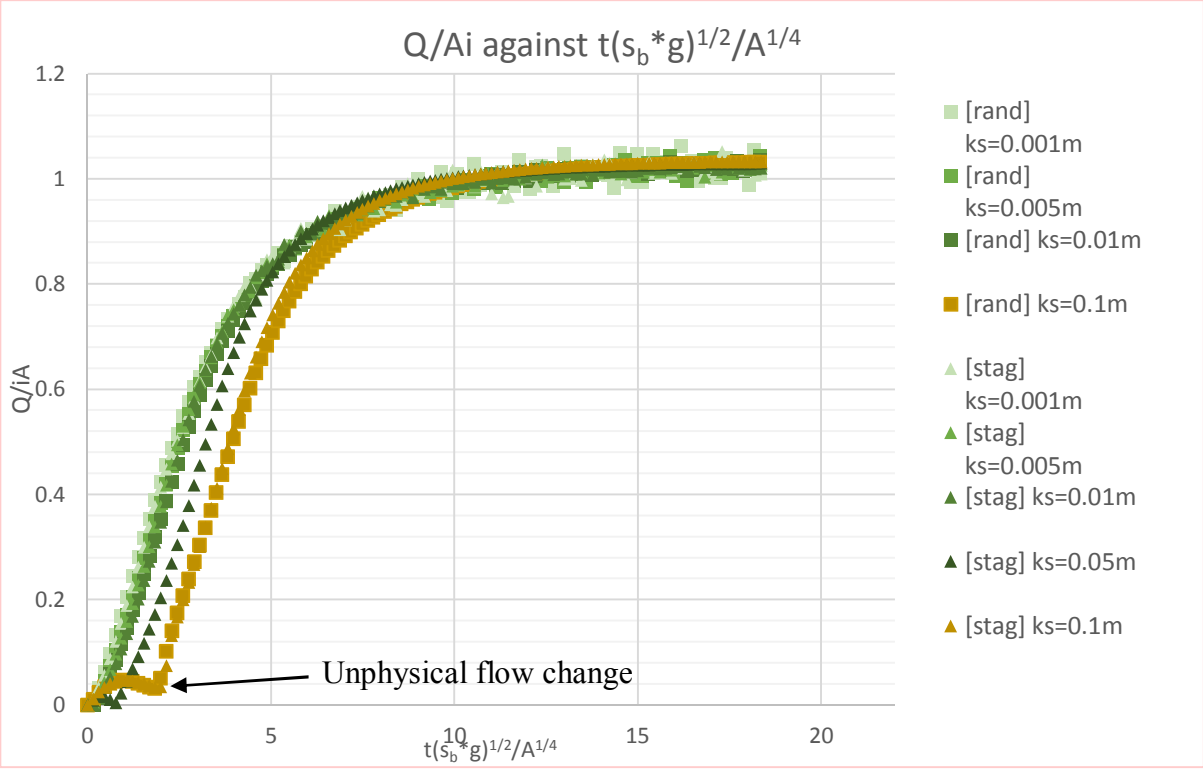

Figure 34 Relationship between dimensionless flow and dimensionless t_{70} (roughness height, random and staggered matrices)

Effects of bed roughness were also tested with roughness height (k_s). The benefit of using k_s was to be able to visualize the size of particles on ground surface. The use of k_s also allowed flows to operate not only in the steady high Reynolds number region, but also in the transition zone. The graph in Figure 34 however showed that flow obtained from k_s were not physical in high k_s. This was because the computer programme converted k_s values into Chezy coefficient with a formula, and the formula ceased to function when k_s was larger than water depth. Very often water depth was only in the order of 10 mm, whereas in studies of k_s values could be set up to 100 mm (0.1 m). To avoid these extremes, Manning coefficient was used instead.

4.3 Flow Field Examination

Times of concentration were shown to increase with bed roughness in Figure 33. In velocity field diagrams, length of arrows indicated the magnitude of velocity. All snapshots in Figure 35 adopted the same colour scale for water depth and same magnification of arrows in indicating velocity. All snapshots were taken at simulation time t=100 seconds, when flow was already saturated. Observing from velocity field diagrams in Figure 35, arrows in $n = 0.001\ m^{\frac{-1}{3}}s$ were larger than arrows in $n = 0.05\ m^{\frac{-1}{3}}s$ in both regular and random matrices. Water depth was also higher in high bed roughness than low bed roughness. Both were evidence showing that increasing bed roughness reduced velocity and lengthened the time of concentration.

Physically the decrease of velocity was due to an increase of friction. Water dissipated more energy through work done on the bed surface, hence lost energy as it flowed towards the end of catchment.

	$n = 0.001\ m^{\frac{-1}{3}}s$	$n = 0.05\ m^{\frac{-1}{3}}s$
Regular Flow Field	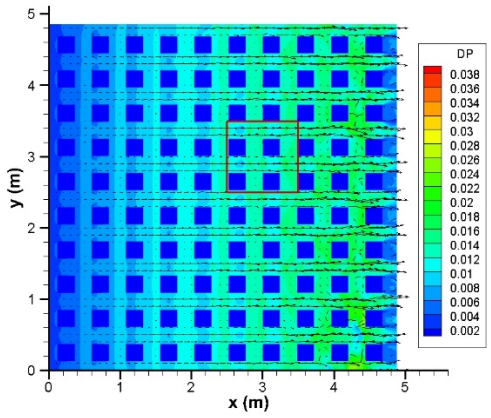	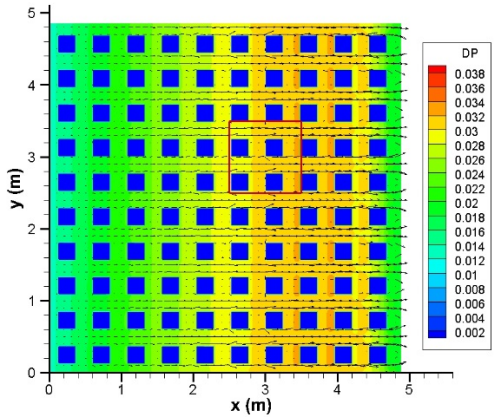
Regular Velocity Field	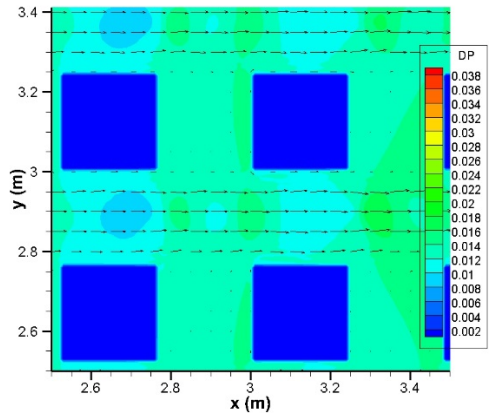	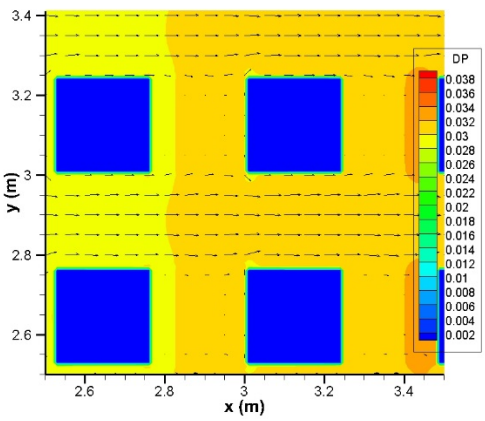
Random Flow Field	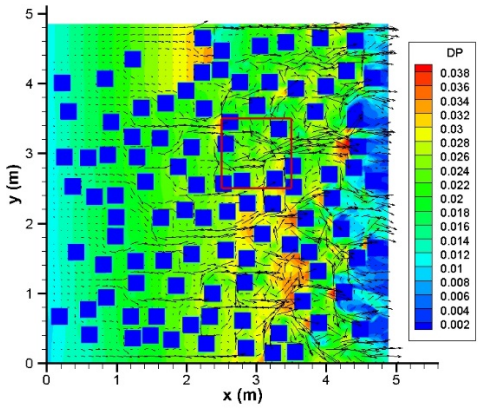	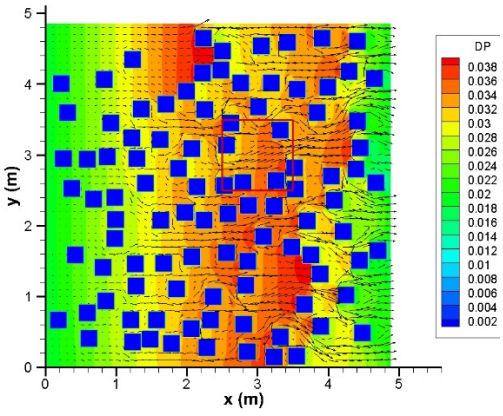
Random Velocity Field	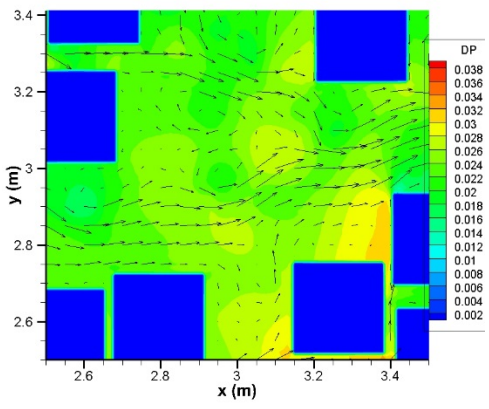	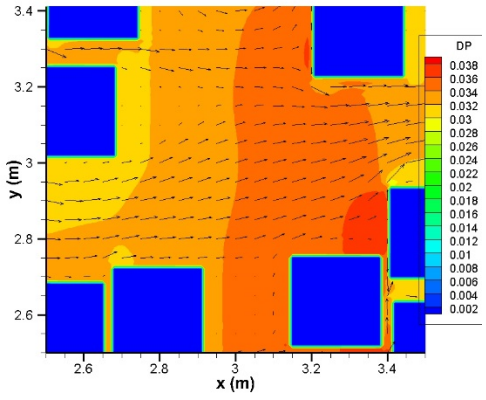

Figure 35 Flow and velocity fields, regular and random matrices on bed roughness

Conclusions

1. Conclusions

Influences of building area ratio, building density and bed roughness to rainfall-induced flooding were studied in the project. This was achieved by simulating rain-induced floods in an in-house computer model based on the TVD-MacCormack scheme.

The project was built on the foundation of multiple theories. The unit hydrograph theory assumed a saturation of outflow to occur at the time of concentration, in response to a continuous uniform rainfall. The two-dimensional shallow water equations with Total Variation Diminishing term allowed flood properties to be calculated. Dimensional analysis enabled results from different topography and rainfall to be generalized.

The model was set up by declaring a number of variables. It was found in previous research that dimensionless terms $\frac{Q_x}{it}$ and $\frac{t\sqrt{s_b \times g}}{A^{\frac{1}{4}}}$ were capable of generalizing flows and time while capturing influences of different rainfall (i), surface gradient (s_b) and catchment area (A). Resolution could be varied to obtain more accurate flow data in a finer mesh. Time step was defined by user and was constrained by the grid size and the maximum velocity of flow. Variables to investigate were the building area ratio, building density, bed roughness and building patterns. Buildings were represented by the building-hole method, proven in previous researches. They were generated by an in-house programme, having the flexibility of altering number of buildings, building pattern (regular, staggered or random), size of buildings and bed roughness.

Flow data was processed after the completion of simulation. By integrating the flow at the outlet of catchment, flow data would be obtained against time. Dimensionless S-curves could then be drawn. The time at which 70% of flow was reached would be recorded, and was benchmarked against different simulations. This was done in view of the theoretical impossibility to simulate 100% flow in computation.

The model was verified in previous research and in this study. It was found that curves of flow in different rainfall and topographic conditions would collapse after adopting the dimensionless terms. This proved that the dimensionless terms were helpful in the research. In addition, it was proven that the choice of resolution and catchment made no statistical differences to the time of concentration obtained.

Influences of building area ratio, building density and bed roughness were analysed through application of the model. It was found in general, that increasing building area ratio,

increasing building density and increasing bed roughness would cause a lengthening time of concentration. The increase was due to a reduced velocity of flow in the catchment. With more buildings, water meandered through more obstacles, losing more energy as it hit the building surface or turned around at corners of buildings. Investigating deeper into the flow field, increasing building area ratio or density would build up the separation layer, narrowing the gaps between buildings. This narrowing made channels not fully utilised. With increasing building area ratio or density, the aggregated effect of channel under-utilisation would be more pronounced; hence the time of concentration increased.

In investigating influence of building area ratio, 0, 5%, 10%, 20% and 30% of catchment area were tested in regular, staggered and random matrices. It was found that the time of concentration increased in linear relationship in regular and random matrices, while it rose in quadratic relationship in staggered matrices. The difference was a result of curve fitting; time of concentration was found to increase more readily in low building area ratio than in high building area ratio in staggered pattern. The time of concentration was lower in low BA in staggered matrix than in random matrices because there were more convolutions and fewer open plains. As the building area increased the opposite effect was observed.

In investigating influence of building density, 25, 36, 64, 100, 144, 225 and 400 buildings were tested in constant topographic and hydrological conditions. Similar to the influence of building area ratio, time of concentration rose linearly in regular and random matrices, but in quadratic relationship in staggered matrices. This was because the lengthening of time of concentration was found to be more readily in low number of buildings than in high number of buildings. The effect was caused by more scattering of buildings so channel was not fully utilized.

In investigating influence of bed roughness, attempts were made to declare roughness in manning coefficient or roughness height. It was found that manning coefficient would give much better flow response. This was because the formula bridging roughness height and Chezy coefficient for Colebrook-White equation broke down when water depth was lower than the roughness height. Unphysical outflow would be resulted when such break down occurred. Manning coefficients were tested in the range of $0.001m^{\frac{-1}{3}}s$ to $0.05m^{\frac{-1}{3}}s$. In all building patterns, times of concentration increased with roughness in linear relationship. They were all found to be greater than results from plain terrain, which was sensible.

2. Future Work

Two directions could be followed from the current progress in the future. Firstly, rectangular catchments could be used instead of the current square ones. Comparisons could be made between results obtained from square catchments and results from rectangular catchments. The combination of rectangular and square geometries would allow many more scenarios to be simulated. This would enhance the adoption of research results in daily design practices.

As part of suggested work in the future, relationships obtained in this project could moreover be used to compare with results from simulations and water table experiments. A matching result would provide a strong evidence proving validity of the research. With careful selection of a small patch in a real rain catchment area, research results could then be adopted to understand how fast would flood saturate under continuous downpour. In view of likely flash floods, analogous to what had happened in urban areas, extra drainage or attempts to return to natural environment could be designed, so that water could flow under the surface and ease flooding pressure. The combination of simulation and lab testing results may boost confidence of future researchers and drainage designers to use research results.

Acknowledgements

This project would not have been completed without assistance from supervisor Dr. Dongfang Liang. His guidance and explanations throughout the project had affirmed the direction of research and improved understanding of what simulation results implied. The provision of opportunity to me also enabled me to have a taste of the research world and know more about urban flooding. Gratitude should also be shown to the Department of Engineering, University of Cambridge and Pembroke College, for the academic guidance and teaching provided throughout my university life.

References

Butler, S. S. (1977). Overland-flow Travel Time Versus Reynolds Number. *Journal of Hydrology*, *32*, 175–182.

Cea, L., Garrido, M., & Puertas, J. (2009). Experimental validation of two-dimensional depth-averaged models for forecasting rainfall-runoff from precipitation data in urban areas. *Journal of Hydrology*, *382*(1-4), 88–102. http://doi.org/10.1016/j.jhydrol.2009.12.020

Gottardi, G., & Venutelli, M. (2007). An accurate time integration method for simplified overland flow models. *Advances in Water Resources*, *31*(1), 173–180. http://doi.org/10.1016/j.advwatres.2007.08.004

Govindaraju, R. S., Kavvas, L., & Jones, S. E. (1990). Approximate Analytical Solutions for Overland Flows. *Water Resources Research*, *26*(12), 2903–2912.

Liang, D., Lin, B., & Falconer, R. (2006). Simulation of rapidly varying flow using an efficient TVD–MacCormack scheme. *International Journal for Numerical …*, (August 2006), 811–826. http://doi.org/10.1002/fld

Liang, D., Özgen, I., Hinkelmann, R., Xiao, Y., & Chen, J. M. (2015). Shallow water simulation of overland flows in idealised catchments. *Environmental Earth Sciences*, *74*(11), 7307–7318. http://doi.org/10.1007/s12665-015-4744-5

United Nations. (2014). *World Urbanization Prospects: The 2014 Revision, Highlights (ST/ESA/SER.A/352)*. (P. D. United Nations, Department of Economic and Social Affairs, Ed.). New York, United States: United Nations. http://doi.org/10.4054/DemRes.2005.12.9

Appendix

1. Risk Assessment Retrospective

As identified in the initial risk assessment, the major risk associated to myself was the health risk caused by prolonged use of computers. This included bad posture when sitting and typing, soreness of eyes under extended duration of exposure to digital screens and lack of physical movement when working over hours. Such risks would be more compounded when deadlines were approaching and the person was psychologically pressured. The risks easily be overlooked in retrospect.

Mitigations had been made throughout the project by phasing out work, during the year and during the day. Outside necessary time of data processing and documentation, time of exposure to computers or sitting was reduced. Regular exercises also allowed muscles to stretch and pressure to relieve. Improvements would enable better care when completing similar projects in the future.

2. Matlab Script for Building Matrix and Terrain Generation

```
%grid parameters
grid_x=281*2;
grid_y=243*2;                  %always smaller than grid_x. Square catchment
with side length grid_y
dx=0.01;
gradient=0.01;              %gradient of catchment
g_domain=dx*gradient;
g_end=dx*gradient*2;        %gradient of leeway is set as twice the
gradient of catchment
friction=1e30;              %friction value at output

% Request the building area and mode of building allocation

prompt = 'Side length of buildings ';
result = input(prompt);
width = result;
width = round(width);

prompt = 'Regular, staggered or random? (1 - regular, 2 - staggered, 3 -
random) ';
result = input(prompt);
fm = result;

% Request no. of rows and columns NOTE ROWS AND COLUMNS FLIPPED IN MATLAB!

if fm==1||fm==2
    prompt = 'Number of columns of buildings (along x axis) ';
    result = input(prompt);
    nc = result;
    prompt = 'Number of rows of buildings (along y axis) ';
    result = input(prompt);
    nr = result;

    % find the number of buildings
    nb = nr*nc;

    % Find the width of gaps (regular and staggered matrix only)
    gx = (grid_y-2-(nr*width))/nr;         %numerator=nc because only gx/2
towards the edge, instead of gx
    gx = round(gx);


else
    prompt = 'Number of square obstacles ';
    result = input(prompt);
    nb = round(result);
end



% Basic grid with edges
a  = ones(grid_x, grid_y);
a(1, 1:grid_y) = 0;
a(grid_x, 1:grid_y) = 0;
a(1:grid_x, 1) = 0;
a(1:grid_x, grid_y) = 0;
```

```
%loop through all of the buildings and set them to zeros
if fm == 1
    for x = 1:nc
        for y = 1:nr
            a(round(gx*(x-0.5)+2+width*(x-1)):round(gx*(x-0.5)+width*x+1),
round(gx*(y-0.5)+2+width*(y-1)):round(gx*(y-0.5)+width*y+1) ) = 0;
        end
    end
elseif fm == 2
    for x = 1:nc,
        for y = 1:nr,
            if mod(x,2) == 0
                for y = 1:nr
                    a(round(gx*(x-0.5)+2+width*(x-1)):round(gx*(x-
0.5)+width*x+1), round(gx*(y-0.5)+2+width*(y-1)):round(gx*(y-
0.5)+width*y+1)) = 0;
                end
            else
                for y = 1:(nr-1)
                    a(round(gx*(x-0.5)+2+width*(x-1)):round(1+gx*(x-0.5) +
width*x), round(gx*y+2+width*(y-0.5)):round(1+gx*y + width*(y+0.5)) ) = 0;
                end
            end
        end
    end

else
    for i = 1:nb
        for k = 1:10000

            %generate random coordinates and limit the end of obstacle be
            %placed within the catchment
            x = ceil((grid_y-width)*rand);
            y = ceil((grid_y-width)*rand);
            x_checkmax = min(x+width,grid_x);
            x_checkmin = max(x-1,1);
            y_checkmax = min(y+width,grid_y);
            y_checkmin = max(y-1,1);

            %check obstacles are not around any existing obstacles and make
            %sure the check box is not outside the catchment area
            if a(x_checkmin:x_checkmax,y_checkmin:y_checkmax)== 1

                %set grids of obstacles = 0
                a(x:x+width-1,y:y+width-1) = 0;
                break

            end
            if k==10000
                disp('Warning: no empty space for new obstacle');
            end

        end
    end
end
```

```
%produce all data in terrain condition
FinalMatrix =[];
domain_end=g_domain*(grid_y-1);

for y=0:1:grid_y-1
    M(1,:)=1:grid_x;
    M(2,:)=1+y;
    for x=1:grid_x
        if a(x,y+1)== 0
            if M(1,x)~=1 & M(1,x)~=grid_x & M(2,y+1)~=1 & M(2,y+1)~=grid_y
                M(3,x)=-10;
            else
                if x<grid_y-1
                    M(3,x)=0+g_domain.*(x-1);
                else
                    M(3,x)=domain_end+g_end.*(x-grid_y);
                end
            end
        else
            if x<=grid_y-1
                M(3,x)=0+g_domain.*x;
            else
                M(3,x)=domain_end+g_end.*(x-grid_y);
            end
        end
    end
    M(4,:)=-M(3,:);
    M(5,:)=0;
    M(6,:)=0;
    M(7,:)=friction;
    M(8,:)=0;
    FinalMatrix=[FinalMatrix M];
end
fileID = fopen('terrain_condition.txt','w');
str=fprintf(fileID,'%d\t %d\t %.8f\t %.8f\t %d\t %d\t %e\t
%d\n',FinalMatrix);

total=sum(sum(a(1:grid_y,:)))
dlmwrite('grid2.out',a, '');
```

3. Data of Random Matrix in Building Area Study (100 Buildings)

Scenario	Time (s)	$\frac{t_{70}\sqrt{s_b \times g}}{\sqrt[4]{A}}$
Building Area 0%	8.30	1.18125
Building Area 5%		
Building Area 5% (1)	11.39	1.64299
Building Area 5% (2)	11.79	1.69993
Building Area 5% (3)	11.46	1.65250
Building Area 5% (4)	12.81	1.84754
Building Area 10%		
Building Area 10% (1)	15.77	2.30067
Building Area 10% (2)	14.29	2.08597
Building Area 10% (3)	15.46	2.25543
Building Area 10% (4)	14.70	2.14573
Building Area 20%		
Building Area 20% (1)	22.84	3.44386
Building Area 20% (2)	22.06	3.32521
Building Area 20% (3)	19.15	2.88636
Building Area 20% (4)	20.54	3.09618
Building Area 20% (5)	19.17	2.88924
Building Area 20% (6)	21.62	3.25889
Building Area 20% (7)	22.27	3.35704
Building Area 30%		
Building Area 30% (1)	27.60	4.30919
Building Area 30% (2)	27.64	4.31675
Building Area 30% (3)	24.92	3.89210
Building Area 30% (4)	28.38	4.43142
Building Area 30% (5)	27.60	4.31053
Building Area 30% (6)	26.38	4.11997
Building Area 30% (7)	27.86	4.35028

mean dimensionless t_{70}	1.71		
S.D. of dimensionless t_{70}	0.09	Compared with mean	
Minimum dimensionless t_{70}	1.64299	Difference	0.06775
Maximum dimensionless t_{70}	1.84754	Difference	0.13680

mean dimensionless t_{70}	2.20		
S.D. of dimensionless t_{70}	0.10		
Minimum dimensionless t_{70}	2.08597	Difference	0.11098
Maximum dimensionless t_{70}	2.30067	Difference	0.10372

mean dimensionless t_{70}	3.18		
S.D. of dimensionless t_{70}	0.23		
Minimum dimensionless t_{70}	2.88636	Difference	0.29318
Maximum dimensionless t_{70}	3.44386	Difference	0.26432

mean dimensionless t_{70}	4.25		
S.D. of dimensionless t_{70}	0.18		
Minimum dimensionless t_{70}	3.89210	Difference	0.35508
Maximum dimensionless t_{70}	4.43142	Difference	0.18424

4. Data of Random Matrix in Building Area Study (64 Buildings)

Scenario	Time (s)	$\frac{t_{70}\sqrt{s_b \times g}}{\sqrt[4]{A}}$
Building Area 0%	8.30	1.18125
Building Area 5%		
Building Area 5% (1)	10.86	1.56651
Building Area 5% (2)	11.15	1.60902
Building Area 5% (3)	10.58	1.52674
Building Area 5% (4)	10.59	1.52810
Building Area 10%		
Building Area 10% (1)	13.27	1.93821
Building Area 10% (2)	13.56	1.98084
Building Area 10% (3)	13.53	1.97536
Building Area 10% (4)	14.78	2.15795
Building Area 20%		
Building Area 20% (1)	17.20	2.58636
Building Area 20% (2)	15.72	2.36454
Building Area 20% (3)	18.96	2.85098
Building Area 20% (4)	21.00	3.15772
Building Area 20% (5)	18.58	2.79450
Building Area 20% (6)	20.45	3.07602
Building Area 20% (7)	20.47	3.07909
Building Area 30%		
Building Area 30% (1)	22.91	3.55964
Building Area 30% (2)	22.23	3.45444
Building Area 30% (3)	23.18	3.60281
Building Area 30% (4)	19.94	3.09898
Building Area 30% (5)	22.67	3.52279
Building Area 30% (6)	22.69	3.52593
Building Area 30% (7)	23.79	3.69671

mean dimensionless t_{70}	1.56			
S.D. of dimensionless t_{70}	0.04	Compared with mean		
Minimum dimensionless t_{70}	1.52674	Difference	0.03086	
Maximum dimensionless t_{70}	1.60902	Difference	0.05143	
mean dimensionless t_{70}	2.01			
S.D. of dimensionless t_{70}	0.10			
Minimum dimensionless t_{70}	1.93821	Difference	0.07488	
Maximum dimensionless t_{70}	2.15795	Difference	0.14486	
mean dimensionless t_{70}	2.84			
S.D. of dimensionless t_{70}	0.29			
Minimum dimensionless t_{70}	2.36454	Difference	0.47963	
Maximum dimensionless t_{70}	3.15772	Difference	0.31355	
mean dimensionless t_{70}	3.49			
S.D. of dimensionless t_{70}	0.19			
Minimum dimensionless t_{70}	3.09898	Difference	0.39549	
Maximum dimensionless t_{70}	3.69671	Difference	0.20224	

5. Data of Random Matrix in Building Density Study

Scenario	Time (s)	$\frac{t_{70}\sqrt{s_b \times g}}{\sqrt[4]{A}}$				
0 Building	8.30	1.18125				
25 buildings (1)	18.79	2.86807	mean dimensionless t_{70}	2.76		
25 buildings (2)	17.78	2.71522	S.D. of dimensionless t_{70}	0.20	Compared with mean	
25 buildings (3)	19.47	2.97258	Minimum dimensionless t_{70}	2.50131	Difference	0.43972
25 buildings (4)	16.38	2.50131	Maximum dimensionless t_{70}	2.97258	Difference	0.03154
64 buildings (1)	19.51	2.97839	mean dimensionless t_{70}	2.94		
64 buildings (2)	18.85	2.87804	S.D. of dimensionless t_{70}	0.04		
64 buildings (3)	19.42	2.96501	Minimum dimensionless t_{70}	2.87804	Difference	0.06300
64 buildings (4)	19.27	2.94270	Maximum dimensionless t_{70}	2.97839	Difference	0.03735
100 buildings (1)	25.53	3.89829	mean dimensionless t_{70}	3.36		
100 buildings (2)	21.74	3.31844	S.D. of dimensionless t_{70}	0.44		
100 buildings (3)	22.16	3.38323	Minimum dimensionless t_{70}	2.82635	Difference	0.53022
100 buildings (4)	18.51	2.82635	Maximum dimensionless t_{70}	3.89829	Difference	0.54171
144 buildings (1)	23.06	3.52066	mean dimensionless t_{70}	3.68		
144 buildings (2)	23.08	3.52393	S.D. of dimensionless t_{70}	0.19		
144 buildings (3)	24.59	3.75375	Minimum dimensionless t_{70}	3.52066	Difference	0.15495
144 buildings (4)	25.57	3.90412	Maximum dimensionless t_{70}	3.90412	Difference	0.22851
225 buildings (1)	26.89	4.10489	mean dimensionless t_{70}	4.06		
225 buildings (2)	27.25	4.15980	S.D. of dimensionless t_{70}	0.25		
225 buildings (3)	24.22	3.69776	Minimum dimensionless t_{70}	3.69776	Difference	0.36229
225 buildings (4)	28.02	4.27774	Maximum dimensionless t_{70}	4.27774	Difference	0.21769
400 buildings (1)	32.51	4.96343	mean dimensionless t_{70}	4.74		
400 buildings (2)	31.68	4.83630	S.D. of dimensionless t_{70}	0.24		
400 buildings (3)	28.82	4.39930	Minimum dimensionless t_{70}	4.39930	Difference	0.33595
400 buildings (4)	31.06	4.74197	Maximum dimensionless t_{70}	4.96343	Difference	0.22818